ISSN: 2160-0392 Volume 10, Number 2, April 2020

Scientific Research Publishing

Advances in Chemical Engineering and Science

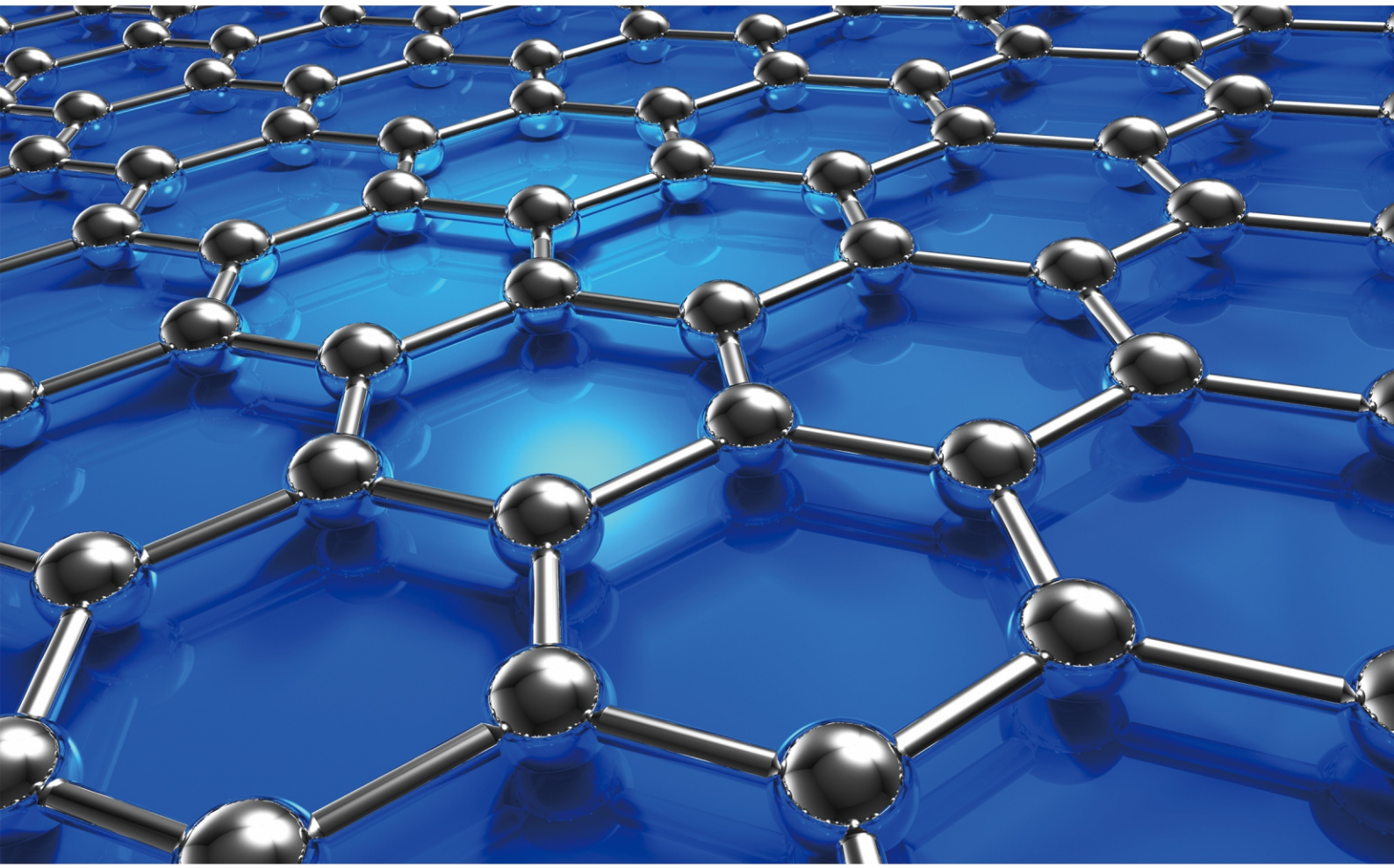

ISSN: 2160-0392

https://www.scirp.org/journal/aces

Journal Editorial Board

ISSN 2160-0392 (Print) ISSN 2160-0406 (Online)
https://www.scirp.org/journal/aces

Editor-in-Chief

Editorial Board

Scientific Research Publishing

Advances in Chemical Engineering and Science, 2020, 10, 81-122
https://www.scirp.org/journal/aces
ISSN Online: 2160-0406
ISSN Print: 2160-0392

Table of Contents

Volume 10 Number 2 April 2020

Advances in Chemical Engineering and Science (ACES)
Journal Information

SUBSCRIPTIONS

The *Advances in Chemical Engineering and Science* (Online at Scientific Research Publishing, https://www.scirp.org/) is published quarterly by Scientific Research Publishing, Inc., USA.

Subscription rates:
Print: $79 per issue.
To subscribe, please contact Journals Subscriptions Department, E-mail: sub@scirp.org

SERVICES

Advertisements
Advertisement Sales Department, E-mail: service@scirp.org

Reprints (minimum quantity 100 copies)
Reprints Co-ordinator, Scientific Research Publishing, Inc., USA.
E-mail: sub@scirp.org

COPYRIGHT

PRODUCTION INFORMATION

For manuscripts that have been accepted for publication, please contact:
E-mail: aces@scirp.org

Scientific Research Publishing

Advances in Chemical Engineering and Science, 2020, 10, 81-98
https://www.scirp.org/journal/aces
ISSN Online: 2160-0406
ISSN Print: 2160-0392

Predictive Models for Optimisation of Acetone Mediated Extraction of Polyphenolic Compounds from By-Product of Cider Production

Salis Ibrahim[1*], Regina Santos[2], Steve Bowra[3]

[1]University for Development Studies, Tamale, Ghana
[2]University of Birmingham, Edgbaston, Birmingham, UK
[3]Department of Research and Development, Phytatec (UK) Ltd., Plas Gogerddan, Aberystwyth, UK
Email: *isalis@uds.edu.gh

How to cite this paper: Ibrahim, S., Santos, R. and Bowra, S. (2020) Predictive Models for Optimisation of Acetone Mediated Extraction of Polyphenolic Compounds from By-Product of Cider Production. *Advances in Chemical Engineering and Science*, **10**, 81-98.
https://doi.org/10.4236/aces.2020.102006

Received: February 9, 2020
Accepted: March 24, 2020
Published: March 27, 2020

Abstract

Response surface methodology (RSM) was applied to provide predictive models for optimisation of extraction of selected polyphenolic compounds from cider apple pomace under aqueous acetone. The design of experiment (DoE) was conducted to evaluate the influence of acetone concentration % (v/v), solid-to solvent ratio % (w/v), temperature (˚C) and extraction time (min) and their interaction on phenolic contents, using the Central Composite Rotatable Design (CCRD). The experimental data were analysed to fit statistical models for recovery of phenolic compounds. The selected models were significant ($P < 0.05$) and insignificant lack of fits ($P > 0.05$), except for Chlorogenic acid and Quercetin 3-glucoside which had significant lack of fits ($P < 0.05$). All models had satisfactory level of adequacies with coefficients of regression $R^2 > 0.9000$ and adjusted R^2_{Adj} reasonable agrees with predicted R^2_{Pri}. Coefficient of variation < 5% for each determination at the 95% confidence interval. These models could be relied upon to achieve optimal concentrations of polyphenolic compounds for applications in nutraceutical, pharmaceutical and cosmetic industries.

Keywords

Cider Apple Pomace, Predictive Models, Optimisation, Polyphenolic Compounds

1. Introduction

Mathematical modelling is an indispensable tool in many applications in science

and engineering. It is the art of translating problems from an application area into tractable mathematical formulations whose theoretical and numerical analysis provides deep understanding to answers and guidance that are useful for originating applications [1]. Mathematical concepts and language are employed to facilitate proper explanation of the system and also explain the effects of different factors, and to make predictions of their behaviour [2]. Modelling based on mathematics provides thorough understanding of the system to be modelled and allows different applications of modern computing capabilities [3]. Models serve as tools for the understanding of very important and complex processes or systems [4]. Different types of models have been proposed and applied in chemical process for optimisation and for designing experiments to give better understanding of complex systems. Response surface methodology (RSM) is a multivariate statistical technique that evaluates the interrelationship between process parameters and responses [5] [6] [7]. Response Surface Methodology was set out by Box *et al.*, 1950 [8] and was a collection of mathematical and statistical techniques used to improve the performance of systems for maximum benefits [9]. By fitting a polynomial equation to an observed data from within a designed of experiment (DoE), the technique was able to predict the behaviour of a response based on the set of independent variables [9]. Response surface methodology provides adequate information from a relatively fewer experimental runs compared to one factor at time procedure which involved plenty of time in experimental trials for model generation. The one factor at a time procedure requires more experiments to be able to explain the interaction of the independent variables on overall dependent quantity or response. Response surface methodology utilises three (3) levels of independent factors to produce experimental designs and employ polynomial models for analysis. RSM has important application in process development, formulation and design of contemporary products in addition to established ones. The technique is widely applicable in chemical and biochemical processes for varied objectives [10]. Comprehensive description of design of experiments by response surface methodology can be obtained from [11] [12] [13].

The current research seeks to demonstrate the possibility of developing predictive models that are reliable for optimisation of the recovery of polyphenolic compounds from cider apple pomace using aqueous acetone as a solvent. Apple pomace is the residue of apple juice and cider production and composed between 20% - 35% by weight of the original production feedstock. The amount of the pomace generated and its composition will depend on the variety of the apple and the techniques used in extracting the juice [14]. Apple pomace is a potential source of carbohydrate, fibre, polyphenolics and pectin [15] [16] which find application in the food, feed, pharmaceutical, cosmetics, chemical, and biofuels sectors [17]. The major polyphenolic compounds found in apples include; Epicatechins, Procyanidins, Phloridzin, Quercetin conjugates and Chlorogenic acids.

2. Materials and Methods

2.1. Apple Pomace

The apple pomace sample composed of 7 varieties of cider apples made of Harry Masters Jersey, Yarlinton Mill, Michelin, Dabinett, Brown Snout, Vilberie and Chisel Jersey, and were collected from Universal Beverages Limited (UBL), Ledbury owned by Heineken international. The apple pomace residues were mixed rigorously to obtain mixture characteristic of the original pomace sample and divided into parts and stored in freezer bags at −20˚C till further investigations.

2.2. Chemical Reagents

All chemical standards and solvents employed in this investigation were ordered at the highest grade of purity from suppliers indicated in the methodologies. Acetonenitrile, and glacial acetic acid were obtained from Fisher Scientific (UK).

2.3. Dry Weight Content of Apple Pomace

A bench top laboratory convention oven (103˚C ± 3˚C) from STATUS International, UK was used for dry weight content. The American Oil Chemist Society (AOCS) standard procedure was utilised to determine the dry matter content, and the results were expressed as the percentage of total fresh weight of the apple pomace as received.

2.4. Apple Pomace Sample Preparation

The apple pomace samples were freeze dried using a vacuum freeze dryer EQ03 (Vacuum and Industrial products). The dried pomace samples from the freeze dryer were placed in desiccator for 30 minutes for samples to return to ambient conditions. Freeze dried pomace residue was pulverised using a domestic Moulinex blender 530 (KEMAEU, France). The blending machine was stopped intermittently after every 20 seconds of milling and the pomace powder packed in dark plastic bags and stored in a cool dry place for subsequent use.

2.5. Extraction of Polyphenolic Compounds from Freeze-Dried Apple Pomace

Known weight of homogenised freeze dried apple pomace was weighed into 100 ml Duran bottles and acetone was added 1% - 8% (w/v) solid-to-solvent ratio and the bottle tightly covered. Extractions were done in an incubator Max Q 4000 series benchtop shaker (Thermo Scientific). Extraction temperatures and time were set and shaking (150 rpm) and automatically stops when extraction time elapses. Extracts rich in polyphenolic compounds were transferred into 50 ml centrifuge tubes and centrifuged in Juan C4 I at 4000 g for 10 minutes. Supernatant volumes were recorded stored at −20˚C. Extractions at 60˚C and 85˚C were done within Grant OLS200 water bath.

2.6. Experimental Design for Optimization of Acetone Mediated Extraction

The design of the experiments was done similar to the procedure previously described in [18]. The design was composed of one factor at a time (OFAT) experiments and the overall design by response surface methodology (RSM). Solvent concentration (%, (v/v)), solid-to-solvent ratio (1% - 8% (w/v)), temperature and extraction time influenced the recovery of polyphenolic compounds. Stat-Ease Design Expert software 7.0, was employed to set up experiments with varying independent variables, utilising the central composite rotatable design (CCRD). In all, thirty (30) experimental runs consisting of 16 trials for factorial points, 8 runs for axial points and 6 duplicates run around the central point (Table 1).

Table 1. Experimental design by central composite rotatable design using 4 factors.

Run order	A-acetone conc. %(v/v)	B-Temp °C	C-Solid/Solvent ratio. % (w/v)	D-Time, min
1	40.0	60.0	1.0	90.0
2	60.0	35.0	1.0	60.0
3	40.0	10.0	8.0	90.0
4	40.0	10.0	1.0	90.0
5	60.0	35.0	4.5	60.0
6	40.0	60.0	8.0	30.0
7	100.0	35.0	4.5	60.0
8	40.0	10.0	8.0	30.0
9	60.0	35.0	4.5	60.0
10	20.0	35.0	4.5	60.0
11	40.0	10.0	1.0	30.0
12	40.0	60.0	8.0	90.0
13	60.0	10.0	4.5	60.0
14	60.0	35.0	11.5	60.0
15	80.0	60.0	8.0	90.0
16	60.0	35.0	4.5	5.0
17	80.0	10.0	8.0	30.0
18	60.0	35.0	4.5	60.0
19	80.0	10.0	8.0	90.0
20	80.0	60.0	1.0	30.0
21	60.0	35.0	4.5	120.0
22	80.0	60.0	1.0	90.0
23	80.0	60.0	8.0	30.0
24	60.0	35.0	4.5	60.0
25	60.0	35.0	4.5	60.0
26	60.0	85.0	4.5	60.0
27	80.0	10.0	1.0	90.0
28	80.0	10.0	1.0	30.0
29	40.0	60.0	1.0	30.0
30	60.0	35.0	4.5	60.0

2.7. Identification and Quantification of Polyphenolic Compounds by High Performance Liquid Chromatography (HPLC)

High performance liquid chromatographic (HPLC) procedure in a reverse mode, previously published in literature was used to separate phenolic compounds [19]. Polyphenolic compounds in extracts were resolved using an Agilent 1100 series HPLC system with DAD-UV detector linked to a Chemstation software. The column used was Prodigy 5 µm ODS3 100A, C18 (250 × 4.6 mm I.D) from Phenomenex (Torrance, CA, USA) with a guard column operated at 40˚C. Eluent A of the mobile phase was composed of 2% (v/v) of glacial acetic acid in water. Eluent B consisted of 0.5% of acetic acid in 50/50 (v/v) of water and acetonitrile. Pure acetonitrile (100%) was the Eluent C. The injection volume was 10 µl per sample and the solvent gradient systems for the separations was as follows: starting with 10% of B and increasing the gradient to 55% B in 50 minutes. Further increase from 55% B to 100% B was done in 10 minutes and finally decreased from 100% B to the initial 10% B in 5 minutes. Eluent C was used to recondition the column under isocratic flow by pumping 100% acetonitrile for 10 minutes, and 10% B also for 10 minutes. The flow rate was 1 ml/min and polyphenolic compounds were monitored at 280 nm for flavanols, 320 nm for hydrocinnamic acid and 370 nm for flavonols. Retention times and spectra data were collected.

2.8. Preparation of Phenolic Standard

Stock solutions (1 mg/ml) of Chlorogenic acid (≥95%), (-) Epicatechin (≥90%), ± Catechin hydrate, Phloridzin dihydrate (≥99%), Procyanidin B2 (≥90%), Quercetin-3-β-D-glucoside (≥90%), Quercetin-3-D-galactoside (≥97%) Phloretin, in Chromasolv for HPLC (Sigma-Aldrich, UK). The stock solutions were diluted appropriately (0.01 - 1 mg/ml) and injected in triplicates into the HPLC equipment. Calibration curves were constructed and quantification of polyphenolic compounds in samples was derived from the calibration curves of corresponding standards.

3. Results and Discussion

The mean dry matter content of the homogenized cider apple pomace under this investigation was 27.7 ± 0.3 g/100g fresh weight. Dry weight value reported for apple pomace in literature ranges, from 21.8 - 33.6 g/100g [20] [21] [22]. Mean dry matter content of the freeze dried apple pomace was 28.3 ± 0.6 g/100g fresh weight.

3.1. Identification and Quantification of Phenolic Compounds in Extracts

The polyphenolic compounds in the extracts were identified by comparing retention times (t_R) and spectra data at maximum absorbance with known phenolic standards. Chlorogenic acid, Caffeic acid, Epicatechin, Procyanidin B, Quer-

cetin-3-galactoside and Quercetin-3-glucoside and Phloridzin, were found to be present in the extracts. These phenolic compounds were identified in industrial apple pomace and documented in literature [4] [19] [23] [24] [25]. The chromatogram of the aqueous acetone extract of the phenolic compounds at 320 nm is shown (Figure 1).

The calibration equations, derived from the plots of concentrations of phenolic standard versus the chromatographic peak areas are shown in Table 2. Concentrations of phenolic compounds (mg/kg) dry weight of apple pomace of various design combinations were obtained from the regression equations of corresponding standards and reported (Table 3).

3.2. Model Selection

A number of modelling options were explored for possible selection, including two factor interactions, quadratic and cubic models. These were tested to select

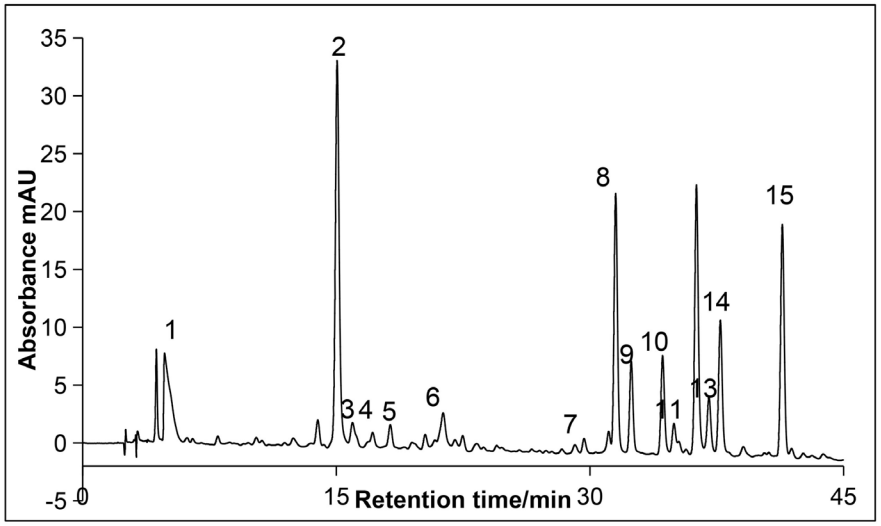

Figure 1. Chromatogram (320 nm) of the extract from the cider apple pomace in aqueous acetone. 1 = solvent peak (acetone), 2 = chlorogenic acid, 3 = procyanidin B2, 4 = caffeic acid, 5 = epicatechin, 7-Ferulic acid, 8 = quercetin-3-galactoside, 9 = quercetin-3-glucoside, 15 = phloridzin.

Table 2. Equations for calibration of standard phenolic compounds from HPLC.

Phenolic Standard	Regression equation	Correlation Coefficient (R^2)
Chlorogenic acid	$y = 25667x$	0.9992
Procyanidin B2	$y = 4.9706x$	0.9833
Quercetin-3-galactoside	$y = 26.232x$	0.9998
Quercetin-3-glucoside	$y = 13829x$	1.0000
Phloridzin	$y = 14704x$	0.9999
Epicatechin	$y = 6210x$	0.9998
Catechin	$y = 5901.3x$	1.0000

Table 3. Concentration of phenolic compounds (mg/kg) dry weight of the cider apple pomace.

Std Order	CGA	PHL	Q-3-gal	Q-3-glu	E-CAT	Pr-B2
1	183.17 ± 4.7	686.35±21.5	159.99 ± 2.4	111.14 ± 2.6	ND	ND
15	170.85 ± 4.0	545.01 ± 10.6	128.88 ± 1.9	89.45 ± 1.7	142.50 ± 9.4	216.85 ± 11.8
19	187.78 ± 7.1	677.32 ± 17.1	171.33 ± 0.5	115.22 ± 3.0	130.30 ± 10.8	201.55 ± 19.8
22	160.99 ± 5.7	562.13 ± 18.9	142.92 ± 4.7	98.83 ± 3.7	132.9 ± 9.7	208.33 ± 1.1
16	201.80 ± 8.7	722.53 ± 25.3	175.09 ± 8.2	117.74 ± 4.7	193.6 ± 33.1	165.80 ± 26.0
23	191.88 ± 5.9	634.49 ± 15.9	174.67 ± 0.4	117.84 ± 2.5	141.5 ± 8.0	227.81 ± 4.4
6	177.39 ± 12.2	641.86 ± 37.7	174.10 ± 12.6	116.91 ± 7.6	173.2 ± 37.9	140.35 ± 28.3
26	190.15 ± 6.8	693.36 ± 20.8	177.78 ± 0.3	118.84 ± 3.3	140.7 ± 10.7	451.69 ± 22.4
14	175.36 ± 7.6	636.60 ± 23.2	173.16 ± 8.1	116.47 ± 4.7	167.4 ± 32.8	150.40 ± 23.3
20	157.05 ± 22.0	776.84 ± 52.9	176.32 ± 18.2	134.37 ± 0.0	ND	ND
11	221.58 ± 9.0	785.27 ± 30.8	186.58 ± 6.1	128.20 ± 2.5	ND	ND
21	184.12 ± 10.9	813.70 ± 31.9	187.83 ± 7.1	131.44 ± 6.7	ND	ND
13	146.69 ± 6.2	484.60 ± 20.6	133.68 ± 5.3	92.88 ± 3.8	132.2 ± 9.1	210.25 ± 5.7
9	167.89 ± 8.7	723.64 ± 36.7	162.88 ± 7.8	114.46 ± 5.9	ND	ND
28	191.38 ± 8.4	713.80 ± 5.7	181.05 ± 1.3	121.81 ± 4.4	152.5 ± 20.0	224.06 ± 3.1
7	162.72 ± 10.6	588.53 ± 6.9	135.03 ± 1.4	93.17 ± 1.2	141.7 ± 5.9	216.38 ± 12.8
18	34.49 ± 4.2	273.55 ± 33.1	30.34 ± 6.5	29.22 ± 0.0	ND	ND
5	156.00 ± 3.5	516.75 ± 12.2	136.02 ± 2.7	94.57 ± 2.1	133.1 ± 6.9	218.26 ± 9.0
25	191.19 ± 5.5	727.07 ± 12.3	176.54 ± 3.3	122.26 ± 2.7	132.5 ± 4.0	217.18 ± 5.4
17	140.67 ± 0.9	314.72 ± 4.2	147.77 ± 0.8	103.45 ± 1.0	109.9 ± 1.6	207.83 ± 10.1
24	191.99 ± 2.9	707.97 ± 18.1	178.16 ± 1.9	119.19 ± 2.2	157.82 ± 10.7	222.60 ± 2.1
12	168.67 ± 14.8	894.62 ± 62.4	172.08 ± 15.4	119.92 ± 0.0	ND	ND
8	190.21 ± 11.3	717.27 ± 28.7	173.37 ± 8.1	116.41 ± 4.3	193.27 ± 19.3	167.11 ± 28.0
30	200.41 ± 3.1	705.85 ± 14.4	182.74 ± 1.6	125.56 ± 1.4	148.98 ± 0.2	225.72 ± 6.0
29	193.29 ± 2.5	709.51 ± 13.0	184.98 ± 1.9	120.09 ± 1.1	142.30 ± 1.8	212.80 ± 0.6
20	248.06 ± 4.7	784.18 ± 20.2	180.15 ± 1.7	120.74 ± 2.1	264.15 ± 30.0	339.78 ± 18.7
10	143.60 ± 13.7	845.59 ± 67.5	164.39 ± 14.0	ND	ND	ND
2	124.51 ± 11.6	847.53 ± 64.9	173.26 ± 11.8	ND	ND	ND
3	189.90 ± 0.9	674.83 ± 44.2	149.79 ± 0.9	104.02 ± 1.4	ND	ND
27	192.57 ± 3.0	682.51 ± 15.8	175.66 ± 1.7	121.14 ± 1.6	138.97 ± 5.2	216.97 ± 3.1

Std = standard, CGA-Chlorogenic acid; PHL-Phloridzin; Q-3-gal-Quercetin-3-galatoside; Q-3-glu-Quercetin-3-glucoside; E-CAT-Epicatechin; Pr-B2-Procyanidin B2; ND not detected.

suitable model that best fits, and capable of depicting the real time response of the surface. For a given model to be appropriate, then it should be significant ($P < 0.05$) and an insignificant lack of fit ($P > 0.05$). Analysis of variance (ANOVA)

at 95% confidence interval were performed utilising Stat-Ease software on the data shown in Table 3, to study the influence of the solvent concentration, solid to solvent ratio, temperature and extraction time on overall recovery of the responses. The results obtained were fitted into a generalised second order polynomial model as in (1):

$$Y = \beta_0 + \sum_{i=1}^{4} \beta_i x_i + \sum_{i=1}^{4} \beta_{ii} x_i^2 + \sum \sum_{i<j=1}^{4} \beta_{ij} x_i x_j \quad (1)$$

where Y is the measured response, β_0 β_i β_{ii} and β_{ij} are regression coefficients for intercept, linear, quadratic and interaction terms respectively and x_i and x_j are coded design variables. Selected models for phenolic compounds were significant ($P < 0.05$) and insignificant lack of fit ($P > 0.05$), except for Chlorogenic acid Quercetin 3-glucoside which had significant lack of fit ($P < 0.05$). All models had satisfactory level of adequacies with coefficients of regression $R^2 > 0.9000$, meaning more than 90% of the data generated can be explained by the predictive models. Adjusted correlation coefficients R_{Adj}^2 reasonable agrees with predicted correlation coefficient R_{Pri}^2. Coefficients of variation were < 5% for each determination at the 95% confidence interval. The yields of polyphenolic compounds were significantly affected by acetone concentration, solid-to-solvent ratio, temperature in addition to their interactions. Summary of the analysis of variance (ANOVA) of quantified phenolic compounds is shown in Table 4.

3.2.1. Predictive Model for Extraction of Chlorogenic Acid

Concentration of Chlorogenic acid in extracts varied from 124.5 to 221.58 mg/kg dry weight of the apple pomace with mean concentration of 176.24 mg/kg. The predictive model in terms of actual factors is shown in Equation (2).

$$\begin{aligned} \text{Chlorogenic Acid} = {} & +100.52918 + 3.21207A + 0.29177B - 6.15519C \\ & + 3.24996 \times 10^{-3} D + 0.24195AC - 0.038655BC + 5.36020 \quad (2) \\ & \times 10^{-3} BD - 0.026760CD - 0.037565A^2 - 0.56300C^2 \end{aligned}$$

Table 4. Significance of design factors and interaction terms on responses.

Response	Significance level ($p < 0.05$)											
	A	*B*	*C*	*D*	*AC*	*AD*	*BC*	*BD*	*CD*	A^2	B^2	C^2
CGA	✓	✓			✓			✓		✓		✓
PHL	✓	✓	✓	✓			✓	✓	✓	✓		✓
Q-gal	✓		✓		✓	✓		✓			✓	
Q-glu	✓	✓	✓		✓					✓		✓
Pr-B2	✓	✓	✓		✓	✓				✓		✓
E-CAT	✓	✓	✓									✓
TPC-HPLC		✓	✓		✓				✓	✓		✓

CGA-Chlorogenic acid; PHL-Phloridzin; Q-gal-Quercetin-galactoside; Q-glu-Quercetin glucoside; Pr-B2-Procyanidin B2; E-CAT-epicatechin; TPC-HPLC-total phenolic content (HPLC); ✓-significant. A-acetone concntration; B-Temperature; C-Solid-to-solvent ratio; and D-extraction time.

Chlorogenic acid is polar within polyphenolic compounds and recovery from plant sources require a certain reasonable level of polarity of the solvent. An increase in temperature from 10˚C to 60˚C for 1% solid-solvent ratio for acetone concentration of 40% (v/v), caused yield of Chlorogenic acid to increase by 14%, but decreases by approximately 20% as concentration of acetone approaches 80% (v/v). concentration of acetone 52% (v/v) at 40˚C was reported as good for recovering Chlorogenic acid from apple pomace [26]. The current investigation revealed 46% (v/v) of acetone at 60˚C as good for extracting Chlorogenic acid from the cider apple pomace. Therefore, decreasing the concentration of acetone and increasing temperature favours yield of Chlorogenic acid. Optimal concentration (206.3 mg/kg dry weight of apple pomace) of Chlorogenic acid was recovered and was within the range (30 - 1766 mg/kg) reported for selected cider apples [23]. The variation of design parameters and Chlorogenic acid is shown in **Figure 2**.

3.2.2. Predictive Model for Extraction of Phloridzin

The concentration of Phloridzin in extracts ranged from 314.7 mg/kg to 894.6 mg/kg. The results were consistent with what has been published previously (25 mg/kg to 1061 mg/kg) of cider apples [23]. The model equation based on the regression analysis in terms of actual factors is shown in Equation (3).

$$\begin{aligned}\text{Phloridzin} = {} & +106.89513 + 21.36305A - 1.01061B - 59.51068C \\ & + 0.81180D + 0.18934BC + 0.016002BD - 0.20193CD \\ & - 0.14966A^2 + 4.52601C^2\end{aligned} \quad (3)$$

Phloridzin concentration increased by 16% at 1% solid –solvent ratio as the acetone concentration was increased to 80% (v/v), and decreased by 24% as solid-solvent ratio approaches 8%. Temperature had minimal effect on the recovery

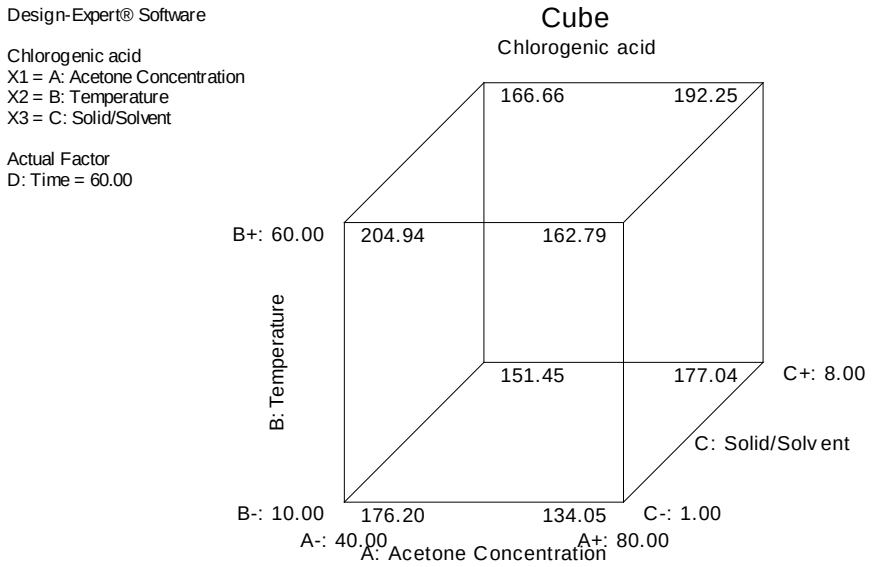

Figure 2. Effects of acetone concentration (% v/v), temperature (˚C) and solid-to-solvent ratio (% w/v) of cider apple pomace on the concntration of Chlorogenic acid (mg/kg) for 60 minute extraction time.

of the dihydrochalcone as it only increased by about 1% when temperature was increased from 10˚C to 60˚C as shown in **Figure 3**.

Optimal concentration of Phloridzin (858.92 mg/kg) was achieved using 73% (v/v) acetone at 60˚C for 60 minutes as against 75% (v/v) at 40˚C for 60 minutes reported earlier [26].

3.2.3. Predictive Model for Extraction of Quercetin Glycosides

Quercetin-3-galactoside dominates among other quercetin glycosides in apple peels [27] and ranged in the extracts from 133.7 - 187.8 mg/kg dry weight of apple pomace with mean concentration of 168.6 mg/kg. Quercetin-3-glucoside ranged in extracts from 60 - 128.2 mg/kg. Both results agreed with previous reports (50 - 520 mg/kg) for Quercetin-3-galactoside, and (9 - 152 mg/kg) of quercetin-3-glucoside in cider apples [23]. Transformed quadratic models excluding outliers were appropriate and described the behaviour of the Quercetin glycosides when the design factors were varied. The model equations are shown in Equation (4) and Equation (5).

$$\begin{aligned}\frac{1.0}{\mathrm{Sqrt}\left(Q-\mathrm{gal}\right)} &= +0.086163-1.15229\times10^{-4}A-3.72357\times10^{-4}B+2.1303710^{-3}C\\ &\quad -6.64449\times10^{-5}D-2.7551\times10^{-5}AC+1.52022\times10^{-6}AD\\ &\quad -1.13192\times10^{-6}BD+6.07617\times10^{-6}B^{2}\end{aligned} \tag{4}$$

$$\begin{aligned}\frac{1.0}{\mathrm{Sqrt}\left(Q-\mathrm{glu}\right)} &= +0.099931-4.32652\times10^{-4}A+1.64815\times10^{-3}C-1.0606\\ &\quad \times10^{-4}D-1.5\times4954610^{-4}AC+1.76547\times10^{-6}AD\\ &\quad +1.06599\times10^{-5}A^{2}+6.69141\times10^{-4}C^{2}\end{aligned} \tag{5}$$

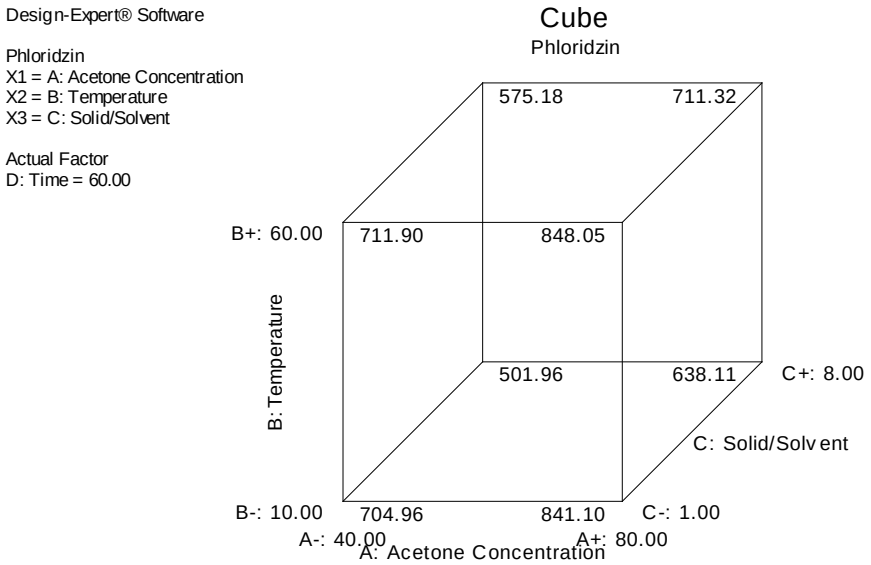

Figure 3. Effects of acetone concentration % (v/v), temperature (˚C) and solid-to-solvent ratio (% w/v) of the cider apple pomace on the concentration of Phloridzin (mg/kg) for 60 minutes extraction time.

Quercetin-3-galactoside concentration increased by 5.24% when concentration of acetone was raised to 80% (v/v) and slightly when temperature increases from 10˚C - 60˚C with increasing solid-to-solvent ratio as reflected in **Figure 4**. Interaction between acetone concentration and solid-to solvent ratio (AC) was more significant than between temperature and time (BD) as revealed by their negative coefficient values which was higher in AC (2.7551×10^{-5}) than BD (1.13192×10^{-6}). The negative coefficient values of temperature and time as well as their interaction suggested overtime with increasing temperature, less recovery of the glycoside could be recovered as shown in **Figure 4**. Decrease in concentration of the glycoside may be due to degradation or hydrolysis of the sugar moieties attached to the quercetin aglycone. Similar results were reported during ultra-sonication procedure of solvent extraction of Quercetin glycosides from "Idared" apple peels [28].

Optimal acetone concentration of 76% (v/v) with 6% solid-to-solvent ratio was good for extracting quercetin-3-galactoside at 41˚C for 58 minutes extraction time. A predicted concentration of 189 mg/kg of quercetin-3-galactoside was suggested for best desirability at the optimal conditions.

Quercentin-3-glucoside showed different behaviour with extraction parameters (**Figure 5**) compared to Quercetin-3-galactoside (**Figure 4**) although both are classified as quercetin glycosides. Both glycosides interacted differently with experimental factors. Solid-to-solvent ratio term influenced positively the yield of quercetin-3-glucoside whereas temperature controlled the elution of quercetin-3-galoctoside in extracts.

The optimal conditions for extracting Quercetin-3-glucoside using aqueous acetone from the apple pomace were 40% (v/v) acetone, 3.5% solid-to solvent

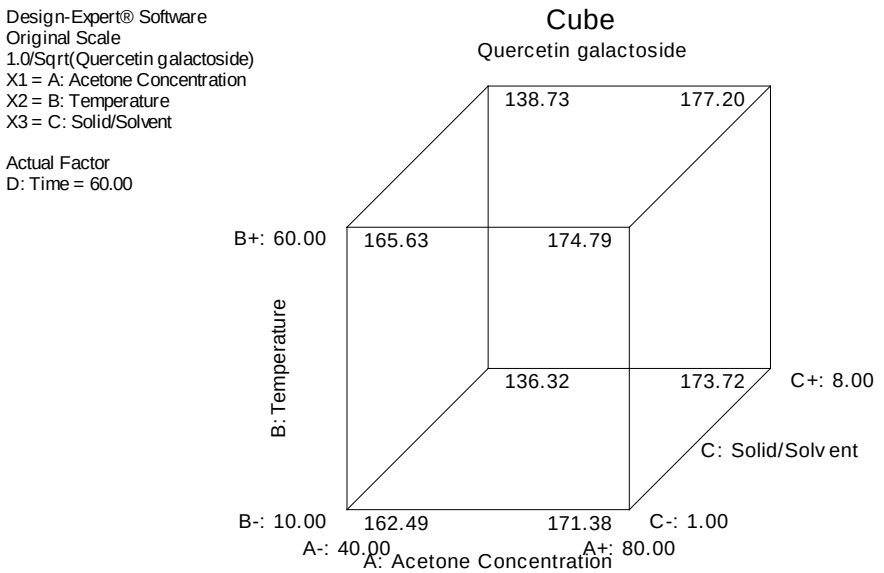

Figure 4. The effects of temperature (˚C), acetone concentration % (v/v) and solid-to-solvent ratio % (w/v) on the concentration of quercetin-3-galactoside (mg/kg) for 60 minutes extraction time.

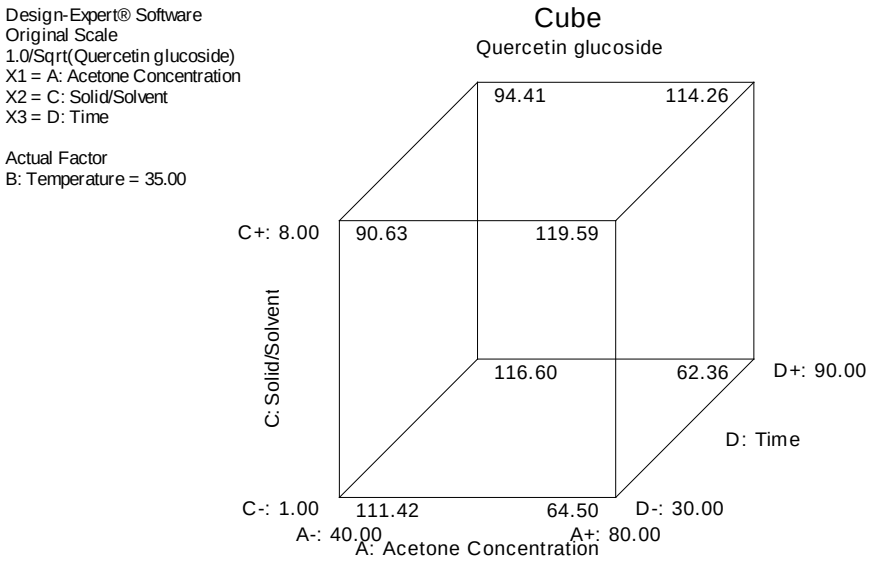

Figure 5. Effects of acetone concentration % (v/v), time (minutes) and solid-to solvent ratio % (w/v) on the concentration of quercetin-3-glucooside at temperature 35˚C.

ratio for 31 minutes at 23˚C extraction temperature. These optimal conditions were different for predicted conditions for recovering quercetin-3-galactoside from the apple peels. It is very important to emphasise that there are no data available in literature to the best of our knowledge as regards good extraction parameters for extracting Quercetin glycosides from cider apple pomace using acetone as an extraction solvent.

3.2.4. Predictive Model for Extraction of Epicatechin

Epicatechin, is a major flava-3-ol, in selected cider apples with concentration in extract ranging from 0 - 193 mg/kg. Similarly, 46 mg/kg to 2225 mg/kg had been reported in fresh cider apples [23]. The regression analysis predicted model equation as shown in Equation (6) and the variation of design parameters with epicatechin concentration shown in **Figure 6**.

$$\begin{aligned}\text{Epicatechin} = &-53.92179 - 0.12460A - 0.037316B + 56.08802C \\ &+ 0.16379AC + 0.051178BC - 5.00284C^2\end{aligned} \quad (6)$$

3.2.5. Predictive Model for Extraction of Procyanidin B2 under Acetone

Molecular and structural differences within Proanthocyannidins make their extraction and quantification very challenging. Their complexation with other non-soluble polymers underestimates their quantification due to incomplete extraction [29]. About 50% - 93% of apple Procyanidins may be retained within cell wall material during processing of apple juice [30]. Procyanidin B2, is a major representative of the various groups of the proanthocyanidins in apple peels [19] and varied in the extract from 0 (not detectable) to 227.8 mg/kg with mean concentration of 137.68 mg/kg. Result was consistent with previous reports (56 mg/kg to 1362 mg/kg) of selected British cider apples [23]. Predicted model equation in terms of actual factors of Procyanidin B2 is shown in Equation (7).

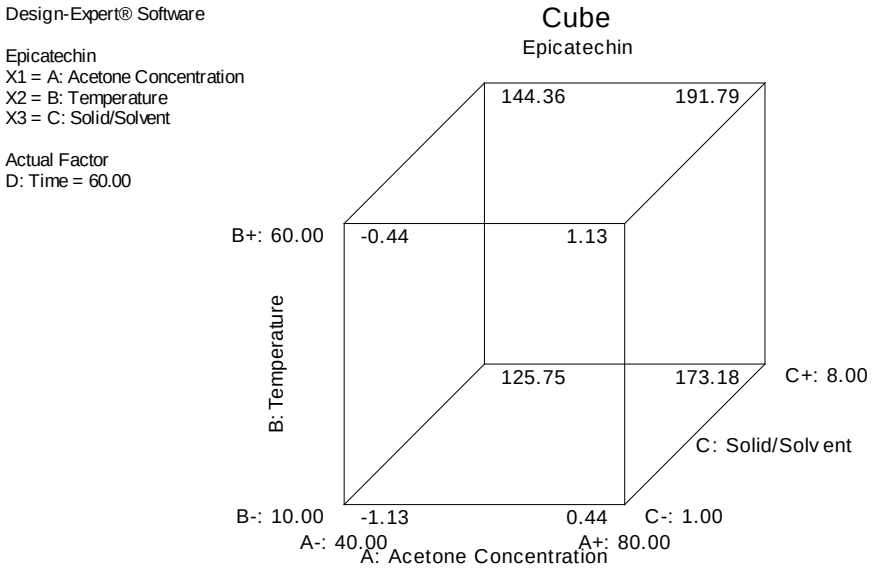

Figure 6. Effects of acetone concentration % (v/v), temperature (˚C) and solid-to-solvent ratio % (w/v) on concntration of epicatechin (mg/kg) dry weight cidr apple pomace for 60 minutes extraction time.

$$\begin{aligned}\text{Procyanidin B2} = &-182.02469 + 2.96978A - 0.011758B + 124.61390C \\ &- 0.35523D - 0.21364AC + 0.034340BC - 0.022831A^2 \\ &- 9.59429C^2 + 2.80355\times 10^{-3}B^2\end{aligned} \quad (7)$$

The variation Procyanidin B2 with experimental factors is shown in **Figure 7**.

The concentration of Procyanidin B2 increases as solid-solvent ratio, temperature and acetone concentration increases and decreases significantly for further increase in these parameters. Optimal solvent concentration and solid-solvent ratio for extracting Procyanidin B2 from the apple pomace at 25˚C for 40 minutes were 54% (v/v) and 6% respectively.

3.3. Effect of Design Variables on Total Phenolic Content by the HPLC Method

Acetone concentration and solid-to solvent ratio and their interaction was the most significant factors in the recovery of the polyphenolic compounds. The model predicted total phenolic content in terms of actual design factors as in Equation (8)

$$\begin{aligned}\text{TPC} = &+320.47139 + 27.34556A - 0.23484B + 42.73751C + 0.66181D \\ &+ 0.67946AC + 0.031083BD - 0.29702CD - 5.91447A^2\end{aligned} \quad (8)$$

The case statistics report showing actual values versus those predicted using the model equation is shown in **Table 5**

The contour plot of the total phenolic content (mg/kg) quantified by HPLC method is shown in **Figure 8**.

Acetone concentration and solid-to-solvent ratio significantly affected the overall yields of extraction of polyphenolic compounds. Optimised conditions of

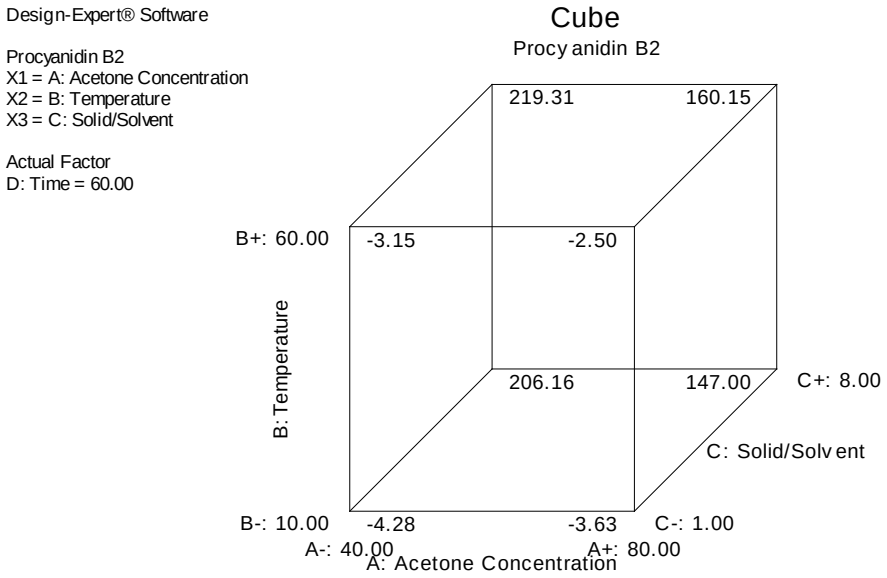

Figure 7. Effect of acetone concentration % (v/v), solid-to-solvent ratio % (w/v) and temperature (˚C) on the amount of Procyanidin B2 (mg/kg) dry weight for 60 minutes extraction time. of apple pomace.

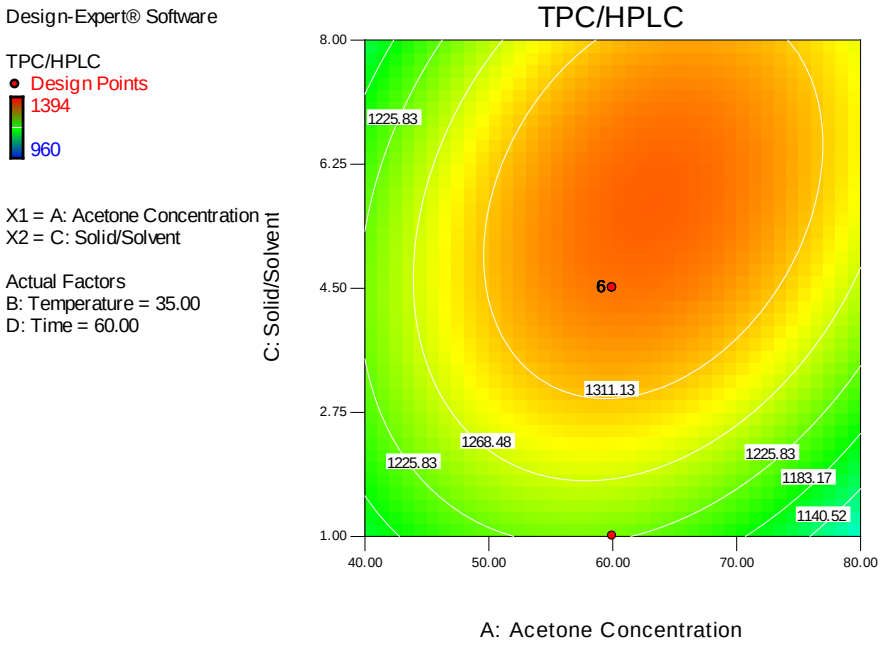

Figure 8. Effect of acetone concentration % (v/v) and solid-to-solvent ratio % (w/v) on total phenolic content (TPC, mg/kg) of acetone extracts of the apple pomace by the HPLC determination

Table 5. Diagnostic case statistics report of total phenolic content (mg/kg) dry weight.

Standard Order	Actual Value (mg/kg)	Predicted Value (mg/kg)	Residual	Leverage
1	1106.00	1101.12	4.88	0.445
2	1044.00	1036.84	7.16	0.470

Continued

3	1043.00	1136.00	−93.00	0.447
4	1103.00	1071.72	31.28	0.469
5	1158.00	1155.55	2.45	0.410
6	1222.00	1281.52	−59.52	0.457
7	1219.00	1190.43	28.57	0.417
8	1303.00	1316.40	−13.40	0.461
9	1120.00	1141.66	−21.66	0.445
10	1046.00	1077.38	−31.38	0.470
11	1314.00	1269.79	44.21	0.447
12	1174.00	1205.51	−31.51	0.469
13	1073.00	1071.34	1.66	0.410
14	1213.00	1197.31	15.69	0.456
15	1109.00	1199.47	−90.47	0.416
16	1366.00	1325.44	40.56	0.460
17	960.00	918.88	41.12	0.73
19	1301.00	1304.06	−3.06	0.145
21	1294.00	1228.78	65.22	0.148
22	1167.00	1142.19	24.81	0.74
23	1300.00	1322.10	−22.10	0.244
24	1340.00	1369.61	−29.61	0.266
25	1354.00	1344.82	9.18	0.097
26	1352.00	1344.82	7.18	0.097
27	1379.00	1344.82	34.18	0.097
28	1360.00	1344.82	15.18	0.097
29	1318.00	1344.82	−26.82	0.097
30	1394.00	1344.82	49.18	0.097

65% (v/v) of acetone, 6% solid-to solvent ratio for 60 minutes at 60˚C were suggested using the statistical model equation with optimal total phenolic content of 1394.01 mg/kg. Validation of the regression model was conducted using the conditions above. The experimental value was determined to be 1392.20 ± 2.9 mg/kg which was in agreement with that predicted by the model.

Higher amounts of phenolic compounds were mobilised around the optimised conditions. The chromatographic methods allowed quantification of individual phenolic compounds present in the extracts without any interference. The HPLC method may not well resolve all phenolic compounds in the extract. For instance, oligomeric flavanols which represent about 71% - 90% of polyphenolic content in apples [31], were not observed in extracts under HPLC used because they might not be retained by the stationary phase.

4. Conclusion

The research demonstrated the application of statistical tools to design experiments for optimisation of recovery of polyphenolic compounds from cider apple pomace using aqueous acetone as solvent. Model equations were generated for selected phenolic compounds by studying the influence of acetone concentration, solid-solvent ratio, temperature and extraction time on extraction of polyphenolic compounds. The independent variables have shown selectivity towards efficient recovery of selected polyphenolic compounds. Improving the polarity of acetone by adding water sufficiently improved recovery of Chlorogenic acid and Procyanidin B2. Quercetin-3-glucoside and Quercetin-3-galactoside exhibited different relationship with temperature and solid-to-solvent ratio although both are classified under Quercetin glycosides. The experimental design predicted 65% (v/v) acetone, 6% (w/v) solid-to-solvent ratio, 60 minutes extraction time at 60˚C as optimum conditions for extracting polyphenolic compounds from the by-product of apple juice and cider production.

Acknowledgements

We acknowledge Universal Beverages Limited (UBL), UK for supplying the cider apple pomace residue and Ghana Education Trust Fund (GETFund) for financial support.

Conflicts of Interest

There are no conflicts of interest as regards this publication.

References

[1] Neumaier, A. (2004) Mathematical Model Building, Chapter 3. In: Kallrath, J., Ed., *Modeling Languages in Mathematical Optimization*, Kluwer, Boston, MA. https://doi.org/10.1007/978-1-4613-0215-5_3

[2] Abramowitz, M. and Stegun, I.A. (1968) Chapter 2-Prediction of Medicinal Properties Using Mathematical Models and Computation and Selection of Plant Materials. *Computational Phytochemistry*, **2018**, 43-73. https://doi.org/10.1016/B978-0-12-812364-5.00002-X

[3] Frejd, P. (2013) Modes of Modelling Assessment—A Literature Review. *Educational Studies in Mathematics*, **84**, 413-438. https://www.jstor.org/stable/43589797

[4] Tauber, M.J. and Ackermann, D. (1991) Mental Models and Human Computer Interaction 2. Elsevier Science Publishers B.V., North-Holland.

[5] Çam, M. and Aaby, K. (2010) Optimization of Extraction of Apple Pomace Phenolics with Water by Response Surface Methodology. *Journal of Agricultural and Food Chemistry*, **58**, 9103-9111. https://doi.org/10.1021/jf1015494

[6] Pinelo, M., Ruiz-Rodriguez, A., Sineiro, J., Reglero, G. and Núñez, M.J. (2007) Supercritical Fluid and Solid-Liquid Extraction of Phenolic Antioxidants from Grape Pomace: A Comparative Study. *European Food Research and Technology*, **226**, 199-205. https://doi.org/10.1007/s00217-006-0526-3

[7] Silva, E., Rogez, H. and Larondelle, Y. (2007) Optimization of Extraction of Phenolics from Inga Edulis Leaves Using Response Surface Methodology. *Separation and*

Purification Technology, **55**, 381-387.
https://doi.org/10.1016/j.seppur.2007.01.008

[8] Gilmour, S.G. (2006) Response Surface Designs for Experiments in Bioprocessing. *Biometrics*, **62**, 323-331. https://doi.org/10.1111/j.1541-0420.2005.00444.x

[9] Bezerra, M.A., Santelli, R.E., Oliveira, E.P., Villar, L.S. and Escaleira, L.A. (2008) Response Surface Methodology (RSM) as a Tool for Optimization in Analytical Chemistry. *Talanta*, **76**, 965-977. https://doi.org/10.1016/j.talanta.2008.05.019

[10] Bas, D. and Boyaci, I.H. (2007) Modeling and Optimization I: Usability of Response Surface Methodology. *Journal of Food Engineering*, **78**, 836-845.
https://doi.org/10.1016/j.jfoodeng.2005.11.024

[11] Box, G.E. and Draper, N.R. (2007) Response Surfaces, Mixtures and Ridge Analyses. 2nd Edition, John Wiley & Sons, New York. https://doi.org/10.1002/0470072768

[12] Gunst, R.F. (1996) Response Surface Methodology: Process and Product Optimization Using Designed Experiments. *Technometrics*, **38**, 284-286.
https://doi.org/10.1080/00401706.1996.10484509

[13] Myers, R.H., Montgomery, D.C. and Anderson-Cook, C.M. (2009) Response Surface Methodology: Process and Product Optimization Using Designed Experiments. John Wiley & Sons, New York.

[14] Shalini, R. and Gupta, D.K. (2010) Utilization of Pomace from Apple Processing Industries: A Review. *Journal of Food Science and Technology*, **47**, 365-371.
https://doi.org/10.1007/s13197-010-0061-x

[15] Cetkovic, G., Canadanović-Brunet, J., Djilas, S., Savatović, S, Mandić, A. and Tumbas, V. (2008) Assessment of Polyphenolic Content and *in Vitro* Antiradical Characteristics of Apple Pomace. *Food Chemistry*, **109**, 340-347.
https://doi.org/10.1016/j.foodchem.2007.12.046

[16] Guyot, S., Marnet, N., Sanoner, P., *et al.* (2003) Variability of the Polyphenolic Composition of Cider Apple (Malus Domestica) Fruits and Juices. *Journal of Agricultural and Food Chemistry*, **51**, 6240-6247.
https://doi.org/10.1021/jf0301798

[17] Sato, M.F., Vieira, R.G., Zardo, D.M., Falcão, L.D., Nogueira, A. and Wosiack, G. (2010) Apple Pomace from Eleven Cultivars: An Approach to Identify Sources of Bioactive Compounds. *Acta Scientiarum Agronomy*, **32**, 29-35.
https://doi.org/10.4025/actasciagron.v32i1.3176

[18] Ibrahim, S., Santos, R. and Bowra, S. (2019) Optimisation of Organic Solvent Mediated Solubilisation of Apple Pomace Polyphenolic Compounds Using Response Surface Methodologies. *International Journal of Chemistry*, **11**, 1-21.
https://doi.org/10.5539/ijc.v11n2p1

[19] Schieber, A., Keller, P. and Carle, R. (2001) Determination of Phenolic Acids and Flavonoids of Apple and Pear by High-Performance Liquid Chromatography. *Chromatography A*, **910**, 265-273. https://doi.org/10.1016/S0021-9673(00)01217-6

[20] Joshi, V.K. and Attri, D. (2006) Solid State Fermentation of Apple Pomace for the Production of Value Added Products. *Natural Product Radiance*, **5**, 289-296.

[21] Kennedy, M., List, D., Lu, Y., Newman, R.H., Sims, I.M, Bain, P.J.S., Hamilton, B. and Fenton, G. (1999). Apple Pomace and Products Derived from Apple Pomace: Uses, Composition and Analysis. Springer, Berlin, Heidelberg.
https://doi.org/10.1007/978-3-662-03887-1_4

[22] Sun, J., Chu, Y.-F., Wu, X. and Liu, R.H. (2002) Antioxidant and Antiproliferative Activities of Common Fruits. *Journal of Agricultural and Food Chemistry*, **50**,

7449-7454. https://doi.org/10.1021/jf0207530

[23] Serena, C.M., William, M. and Crozier, A. (2007) Flavonoids and Chlorogenic Acid Profiles of English Cider Apples. *Journal of the Science of Food and Agriculture*, **87**, 719-728. https://doi.org/10.1002/jsfa.2778

[24] Diñeiro, G.Y., Valles, B.S. and Picinelli, L.A. (2009) Phenolic and Antioxidant Composition of by-Products from the Cider Industry: Apple Pomace. *Food Chemistry*, **117**, 731-738. https://doi.org/10.1016/j.foodchem.2009.04.049

[25] Suarez, B., Ángel L. Álvarez, Yolanda Diñeiro García, de Barrio, G. Lobo, A. P., & Porra, F. (2010) Phenolic Profiles, Antioxidant Activity and *in Vitro* Antiviral Properties of Apple Pomace. *Food Chemistry*, **120**, 339-342. https://doi.org/10.1016/j.foodchem.2009.09.073

[26] Wijngaard, H.H. and Brunton, N. (2010) The Optimisation of Solid–Liquid Extraction of Antioxidants from Apple Pomace by Response Surface Methodology. *Journal of Food Engineering*, **96**, 134-140. https://doi.org/10.1016/j.jfoodeng.2009.07.010

[27] Tsao, R. and McCallum, J. (2009) Chemistry of Flavonoids. Blackwell Publishing, Ames, IA.

[28] Vasantha Rupasinghe, H.P., Kathirvel, P. and Huber, G.M. (2011) Ultrasonication-Assisted Solvent Extraction of Quercetin Glycosides from 'Idared' Apple Peels. *Molecules*, **16**, 9783. https://doi.org/10.3390/molecules16129783

[29] Pérez-Jiménez, J., Arranz, S. and Saura-Calixto, F. (2009) Proanthocyanidin Content in Foods Is Largely Underestimated in the Literature Data: An Approach to Quantification of the Missing Proanthocyanidins. *Food Research International*, **42**, 1381-1388. https://doi.org/10.1016/j.foodres.2009.07.002

[30] Le Bourvellec, C. and Renard, C. (2012) Interactions between Polyphenols and Macromolecules: Quantification Methods and Mechanisms. *Critical Reviews in Food Science and Nutrition*, **52**, 213-248. https://doi.org/10.1080/10408398.2010.499808

[31] Vrhovsek, U., Rigo, A., Tonon, D. and Mattivi, F. (2004) Quantitation of Polyphenols in Different Apple Varieties. *Journal of Agricultural and Food Chemistry*, **52**, 6532-6538. https://doi.org/10.1021/jf049317z

Advances in Chemical Engineering and Science, 2020, 10, 99-112
https://www.scirp.org/journal/aces
ISSN Online: 2160-0406
ISSN Print: 2160-0392

Zirconia Modified Pd Electrocatalysts for DFAFCs

Yuh-Jing Chiou[1*], Mao-Yuan Chen[1], Yi-Lan Chang[1], Hong-Ming Lin[2], Andrzej Borodzinski[3]

[1]Department of Chemical Engineering and Biotechnology, Tatung University, Taiwan
[2]Department of Material Science, Tatung University, Taiwan
[3]Institute of Physical Chemistry, Polish Academy of Sciences, Warsaw, Poland
Email: *chiou@gm.ttu.edu.tw

How to cite this paper: Chiou, Y.-J., Chen, M.-Y., Chang, Y.-L., Lin, H.-M. and Borodzinski, A. (2020) Zirconia Modified Pd Electrocatalysts for DFAFCs. *Advances in Chemical Engineering and Science*, **10**, 99-112.
https://doi.org/10.4236/aces.2020.102007

Received: February 17, 2020
Accepted: April 14, 2020
Published: April 17, 2020

Abstract

In order to enhance the Pd based anodic catalysts for direct formic acid fuel cells (DFAFCs), the research work includes increasing catalyst activity and preventing CO poison. In this study, various zirconium oxides-modified multi-walled carbon nanotubes (MWCNTs) were prepared as the supports of Pd catalysts for DFAFCs by adjusting the preparation parameters: metal adding, sintering temperature and atmospheres. The prepared pure zirconia has both monoclinic and tetragonal phases. The addition of MWCNTs depresses the growth of monoclinic phase. A small amount of Pd adding allows both monoclinic and tetragonal zirconia structures to appear again. Pd nanoparticles of 20 wt% synthesized on MWCNTs and tetragonal ZrO_2/MWCNTs have similar particle size, while Pd/[Pd:ZrO_2/AO-MWCNTs-300Air-900Ar] have more nanoparticles aggregation. The electrochemical surface area can be improved by adding zirconia which implies those zirconia modified Pd catalysts better electrocatalytic performance. By analyzing the maximum current density and the corresponding potential, Pd/AO-MWCNTs are inferred to undergo the formic acid direct oxidation initially. The Pd catalysts modified by tetragonal ZrO_2 have higher current density. Those having both tetragonal and monoclinic ZrO_2 modified Pd catalysts have lower potential of formic acid oxidation. All the Pd based catalysts with zirconia modification possess better CO resist ability and electrocatalytic activity.
Pd/[ZrO_2/AO-MWCNTs-300Air-900Ar] and
Pd/[Pd:ZrO_2/AO-MWCNTs-300Air-900Ar] which catalyze formic acid in direct oxidation path are the two best catalysts.

Keywords

DFAFCs, Dual Path, Zirconia, Pd, MWCNTs

1. Introduction

For the topic of clean and renewable energy, fuel cell is an expectable choice: no noise, no charge need, and not depending on weather. People research different types of fuel cells for transportation, stationary power and small electric devices. The basic physical structure of fuel cell consists of an electrolyte layer in contact with an anode (negative electrode) and a cathode (positive electrode). The fuel is fed to anode and oxidized, and oxygen is fed to cathode and reduced. Depending on the electrolyte, fuel cells can be divided into: alkaline fuel cells (AFCs), proton exchange membrane fuel cells (PEMFCs), phosphoric acid fuel cells (PAFCs), molten carbonate fuel cells (MCFCs) and solid oxide fuel cells (SOFCs). Direct methanol fuel cells (DMFCs) have high volumetric energy density (4900 $Wh{\cdot}L^{-1}$) but high fuel crossover through Nafion® membrane. Methanol has the well-known inherent toxicity at vapor phase. Formic acid is nontoxic, nonflammable, with high theoretical open circuit voltage (OCV) at room temperature (25˚C), and low fuel crossover through PEM due to the electrostatic repulsion between $HCOO^-$ of formic acid and SO_3^- ions of the membrane. Although direct formic acid fuel cells (DFAFCs) have the lower volumetric energy density (2104 $Wh{\cdot}L^{-1}$) than DMFCs, it can be overcome via using higher formic acid concentration [1] [2] [3] [4]. It had been studied that the oxidation of formic acid had two reaction pathways at the anode: the direct dehydrogenation and the indirect dehydration in 0.25 - 0.4 V and 0.5 - 0.6 V, respectively [2] [3]. The direct dehydrogenation pathway directly converts formic acid into carbon dioxide (CO_2). The indirect dehydration pathway has partial oxidation of formic acid to form CO intermediate adsorbing on the catalysts surface. The adsorbed CO may poison the catalyst or conduct further oxidation to CO_2.

The anodic catalyst research work is to increase the formic acid oxidation current, which may promise the higher electric power, and to prevent Pd poisoned by CO. Many literatures show that Pd performance can be enhanced by depositing on carbon nanotubes (CNTs) for the well dispersion and CNTs as good chemical promoter [5] [6] [7] [8] [9]. Some studies prepared graphite and carbon nanotubes as expanded surface to deposit Pd [7], developed a shorter-time process to oxidize MWCNTs as the support which increased Pd activity [8], or prepared CNT supported Pd with various metals: Co, V, Mn and Zn by using NaBH4 reduction method [9]. Our group had investigated different modifications to enhance the catalyst performance, such as coating CNTs with conductive polymer to enhance the electro conductance [10] or metal oxide for CO resistance [11] [12] [13] [14]. For transition metal oxide modification, our works include tungsten oxide which has hydrogen spillover effect [12], cerium oxide with metal doping which decrease the CO oxidation temperature and enhance the Pd performance [13], and nitrogen doped titanium oxide which improved the electric conductivity [14]. So the electrocatalytic performance is improved by the modifications.

Zirconia has several advantages such as excellent thermal stability, nontoxicity, and low cost. Zirconia is known to have three low-pressure structural phases:

monoclinic (<1440˚C), tetragonal (1440˚C - 2640˚C) and cubic (>2640˚C) [15] [16] [17]. Tetragonal zirconia is promised to have better oxygen supporting ability under high temperature. Lesiak *et al.* studied ZrO_2 modified MWCNTs as the supports of AuPd catalysts for DFAFCs [18]. They found that ZrO_2 adding can enhance the catalyst activity while the AuPd solid solution contributes the stability. Zirconia in monoclinic phase may be oxygen deficient [19]. As CO adsorbing, CO and zirconia can form a linear structure [20]. This study is to develop optimal prepared zirconia to modify CNTs supports and find the effect for Pd electrocatalytical performance.

2. Experiment Procedures

2.1. Sample Preparation

The supporters were prepared as following. The pristine multiwalled carbon nanotubes (MWCNTs, Yong-Zhen Techno material CO., LTD, China. Purity 98% - 99%) were first acidized by nitric acid to remove the impurity and to form some functional group to benefit the nanoparticles deposition. Then 20 wt% zirconia were synthesized on the acid oxidized MWCNTs (AO-MWCNTs) via solgel method and followed by different sinter atmosphere (air or Ar) and temperature (700˚C or 900˚C). Some zirconia was added by 1 wt% Pd to change the structure of zirconia.

Pd electrocatalysts were deposited on the prepared supporters via x-ray photosynthesis about 8 minutes. The X-ray irradiation experiments were performed at the beamline 01A in National Synchrotron Radiation Research Center (NSRRC), Hsinchu, Taiwan. The parameters of storage ring were 1.5 GeV and 200 mA. Un-monochormatic "white" X-ray beam was utilized throughout the exposure. After the Pd based products centrifuged and dried at 85˚C, the nanoparticles were sintered in 5 mol% H_2/Ar at 200˚C for 1 hour. Finally, Pd/AO-MWCNTs, Pd/ZrO_2/AO-MWCNTs, and Pd/(Pd:ZrO_2/AO-MWCNTs) were obtained in the process above.

2.2. Characterization and Electrocatalytical Performance

The structure and morphology of the prepared samples were determined by XRD, FESEM and TEM. The metal contents of the samples were confirmed by Inductively Coupled Plasma Optical Emission Spectrometer (ICP-OES, Perkin Elmer Optima-2000 DV). Electrochemical activities of catalysts were characterized by cyclic voltammetry (C-V) measurement by adopting a three-electrode system and CHI Instrument Model 6081C potentiostat/galvanostat instrument. Three-electrode cell system is composed by a working electrode (SE100-Carbon Single Electrode SPE, Zensor R&D Co., Ltd., working diameter 0.5 cm, area 0.196 cm^2), a Pt net counter electrode and a Ag/AgCl reference electrode. The measured current was normalized by the Pd weight loaded on the working electrode. During each C-V experiment, the dissolved gas, oxygen, CO or CO_2, was removed from the solution by purging Ar before and during the experiment. In order to observe the resistance of CO, the prepared Pd catalysts working elec-

trode were purged by CO gas for 5 minutes at a flow rate of 10 ml/min, and then kept in CO atmosphere for 30 minutes. The procedure served enough CO to poison Pd/AO-MWCNTs. The poisoned working electrodes were then conducted the CV test.

3. Results and Discussion

The results of characterization and electrocatalytical performance of the prepared Pd based catalysts are discussed below. In Figure 1, the structure of the prepared different zirconia can be first compared in (a). The zirconia has both tetragonal and monoclinic phases as treated under Ar at 700˚C. As the heat treatment temperature increase, tetragonal phase can be depressed and there only exists monoclinic zirconia. However, as carbon nanotubes adding, zirconia only has tetragonal phase. As 1 wt% Pd adding in the ZrO_2/MWCNTs process, the second pattern in (b), there are both monoclinic and tetragonal zirconia phases. The synthesis of 20 wt% Pd on the Pd:ZrO_2/MWCNTs supporter, the first pattern in (b), causes less monoclinic zirconia with tetragonal phase. Even Pd:ZrO_2/MWCNTs supporter after high temperature treatment, monoclinic zirconia on MWCNTs is unstable during the Pd synthesis process. The 20 wt% Pd on the tetragonal zirconia modified MWCNTs supporters, the lower three patterns in (b), doesn't change zirconia structure. The prepared Pd catalysts on different supporters, MWCNTs, three tetragonal zirconia/MWCNTs in different heat treatment conditions, and Pd:ZrO_2/MWCNTs with tetragonal and monoclinic zirconia phases, will be studied below.

Figure 2 shows the FESEM morphology of the prepared Pd catalysts. AO-MWCNTS has average diameter about 17 nm which can be kept constant as Pd or ZrO_2 synthesized on the surface. The images of (b) to (f) show Pd synthesized on different supporters. Grey and black particles can be observed dispersing on the carbon nanotubes surface and recognized as ZrO_2 and Pd nanoparticles, respectively. For Pd/[Pd:ZrO_2/AO-MWCNTs-300Air-900Ar] in (f), more aggregation is observed. As the morphology observing in high resolution TEM

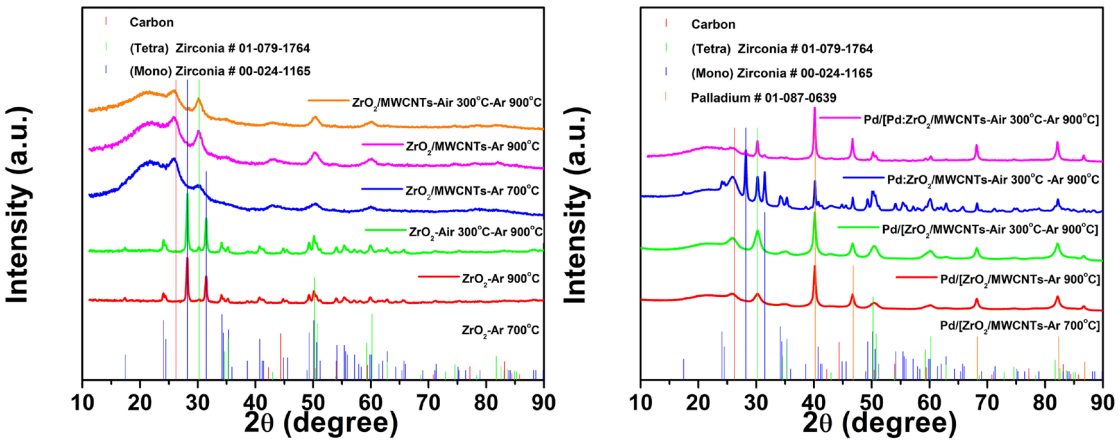

Figure 1. XRD patterns of (a) the prepared zirconia, (b) the prepared Pd catalysts.

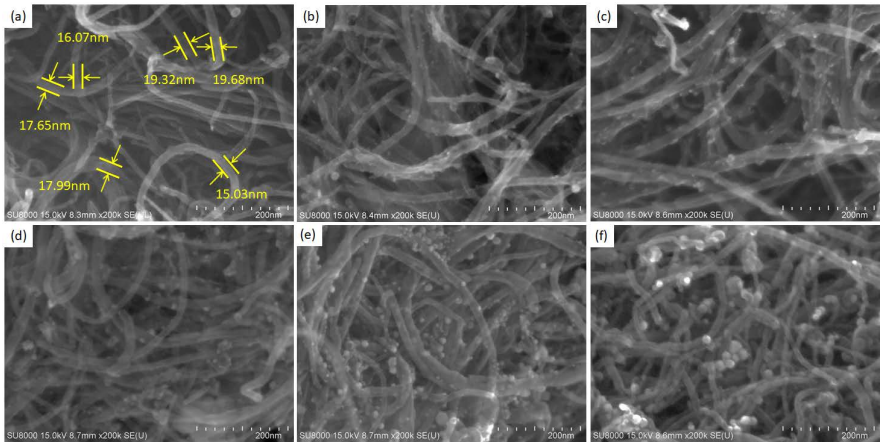

Figure 2. FESEM images of (a) AO-MWCNTs, (b) Pd/AO-MWCNTs, (c) Pd/[ZrO_2/AO-MWCNTs-700Ar], (d) Pd/[ZrO_2/AO-MWCNTs-900Ar], (e) Pd/[ZrO_2/AO-MWCNTs-300Air-900Ar], (f) Pd/[Pd:ZrO_2/AO-MWCNTs-300Air-900Ar].

and analyzing the particle size distribution, all the Pd based nanocomposites look similar. **Figure 3**, the TEM image and particle size distribution of Pd/[ZrO_2/AO-MWCNTs-Air300-Ar900], is a typical image. The smaller grey particles as zirconium oxide and the larger black ones as Pd metal can be recognized. The particle size distribution shows two peaks as smaller zirconia (~3 nm) and larger Pd (~8 nm). As recalling the XRD patterns and estimating the particle size via Sherrer's formula, the results are ZrO_2 as 6.8 nm, Pd as 14.3, 17.6, 19.0, 15.3 and 27.6 nm for Pd/AO-MWCNTs, Pd/[ZrO_2/AO-MWCNTs-700Ar], Pd/[ZrO_2/AO-MWCNTs-900Ar], Pd/[ZrO_2/AO-MWCNTs-300Air-900Ar], and Pd/[Pd:ZrO_2/AO-MWCNTs-300Air-900Ar], respectively. The trend is consistent to the observation of microscope. Though the nanoparticle size in TEM seems similar in nano scale, Pd/[Pd:ZrO_2/AO-MWCNTs-300Air-900Ar] may have more nanoparticles combination.

For the electrocatalytical performance, the catalysts were prepared as a working electrode, and conducted the CV test in sulfuric acid to measure the electrochemical surface area (ECSA) of the Pd catalysts as shown the results in **Figure 4(a)**. Pd/[Pd:ZrO_2/AO-MWCNTs-300Air-900Ar] (45.2 m^2/gPd) which has both monoclinic and tetragonal phases, has a little improved ECSA value from Pd/AO-MWCNTs (43.6 m^2/gPd). The larger Pd particle size can decrease the specific surface area, but zirconia modification may compensate via preventing Pd poisoned. The three Pd/[ZrO_2/AO-MWCNTs]'s with tetragonal zirconia modified Pd catalysts have enhanced the hydrogen adsorption ability more. Their ECSA values are 61.9, 64.4 and 58.1 m^2/gPd for Pd/[ZrO_2/AO-MWCNTs-700Ar], Pd/[ZrO_2/AO-MWCNTs-900Ar], and Pd/[ZrO_2/AO-MWCNTs-300Air-900Ar], respectively. The adding of zirconia does enhance the acid adsorption ability of Pd.

Figures 4(b)-(f) show the CV results of the prepared catalysts oxidizing formic acid in various cycles. Pd/AO-MWCNTs in (b) initially has a big peak at 0.4 V and a minor peak at 0.75 V for direct and indirect formic acid oxidation.

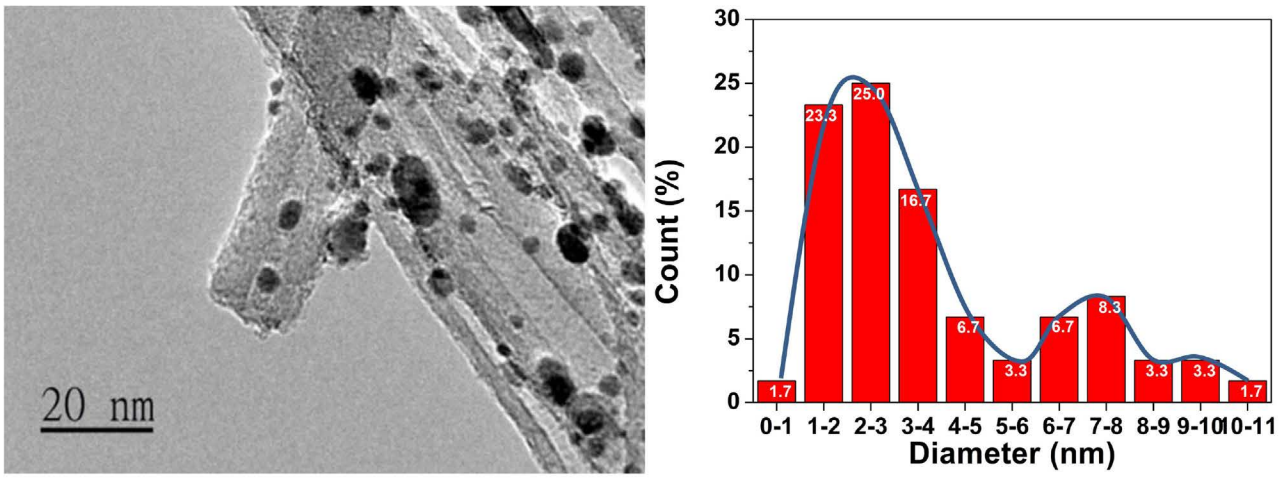

(a) (b)

Figure 3. TEM image and particle size distribution of Pd/[ZrO_2/AO-MWCNTs-Air300-Ar900].

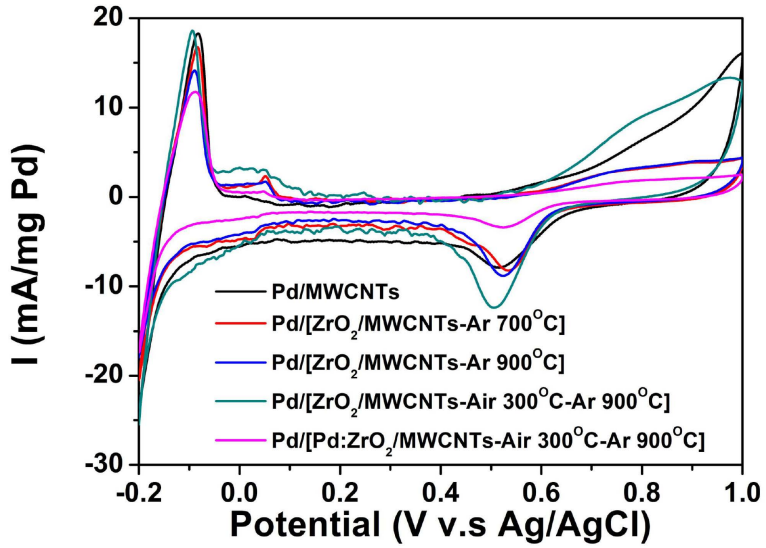

(a)

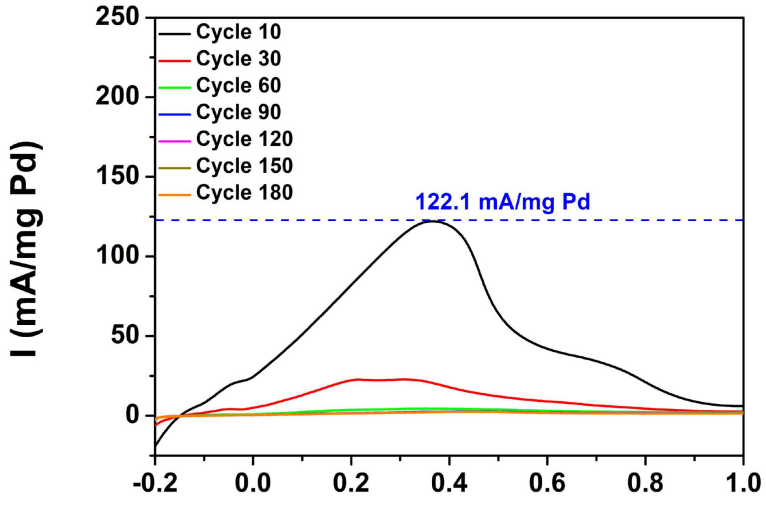

(b)

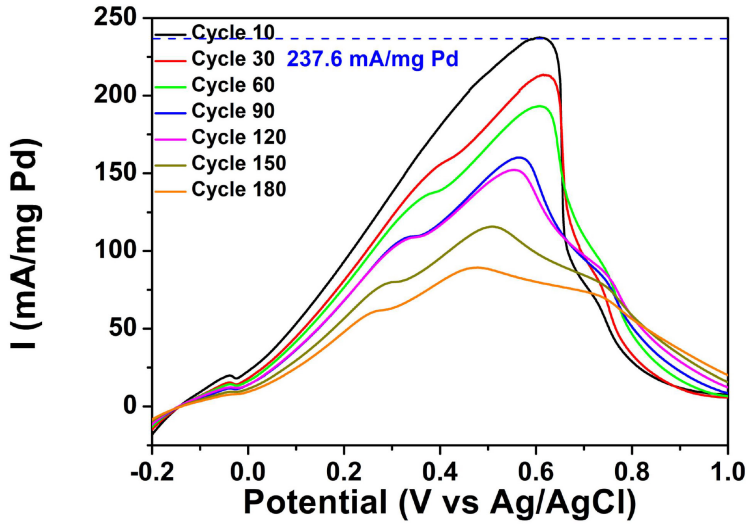
Cycle 10
Cycle 30
Cycle 60
Cycle 90
Cycle 120
Cycle 150
Cycle 180
237.6 mA/mg Pd
I (mA/mg Pd)
Potential (V vs Ag/AgCl)

(c)

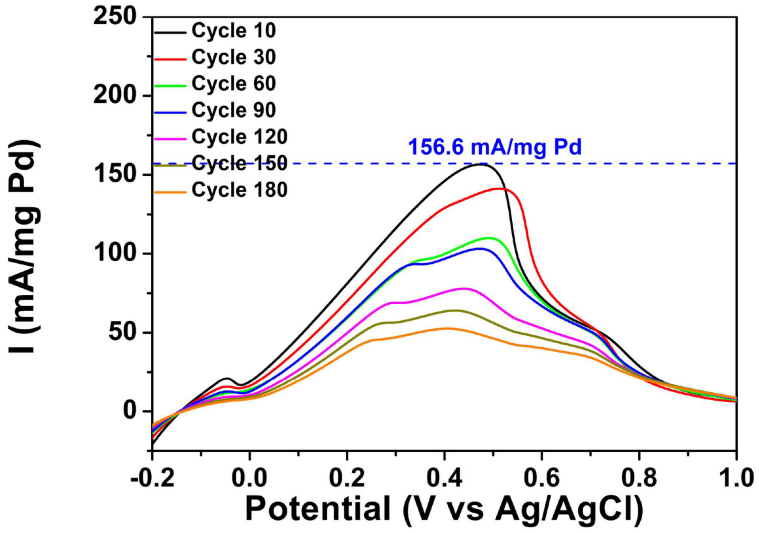
Cycle 10
Cycle 30
Cycle 60
Cycle 90
Cycle 120
Cycle 150
Cycle 180
156.6 mA/mg Pd
I (mA/mg Pd)
Potential (V vs Ag/AgCl)

(d)

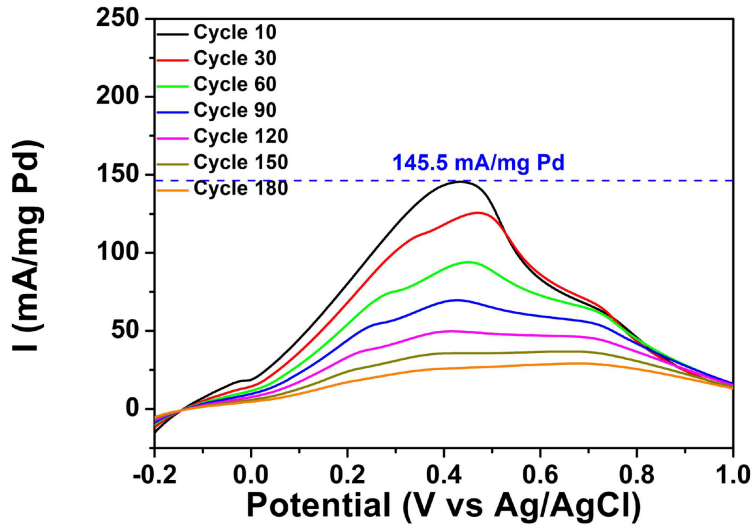
Cycle 10
Cycle 30
Cycle 60
Cycle 90
Cycle 120
Cycle 150
Cycle 180
145.5 mA/mg Pd
I (mA/mg Pd)
Potential (V vs Ag/AgCl)

(e)

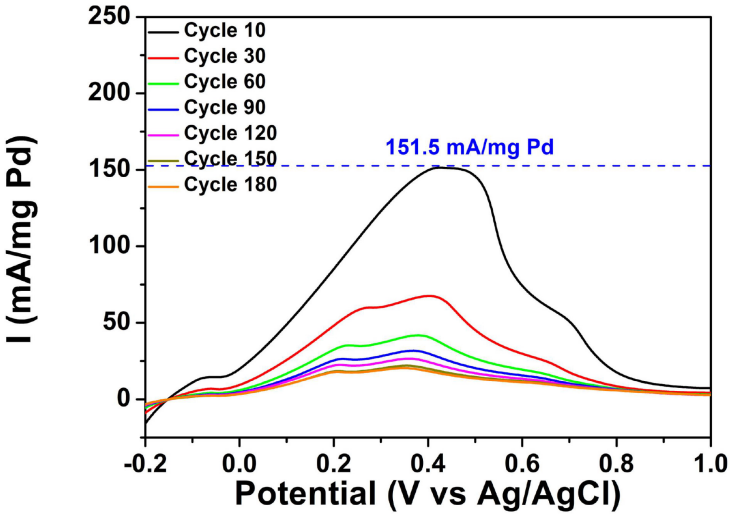

(f)

Figure 4. (a) ECSA plots of Pd catalysts in 1M H_2SO_4, and CV plots of (b) Pd/AO-MWCNTs, (c) Pd/[ZrO_2/AO-MWCNTs-700Ar], (d) Pd/[ZrO_2/AO-MWCNTs-900Ar], (e) Pd/[ZrO_2/AO-MWCNTs-300Air-900Ar], (f) Pd/[Pd:ZrO_2/AO-MWCNTs-300Air-900Ar] in 3M HCOOH and 1M H_2SO_4. Scan rate 10 mV/s.

The activity decays fast. As AO-MWCNTs modified by zirconia, no matter what the preparing parameters are, the activity and stability of formic acid oxidized by the Pd based electrocatalysts are improved. Pd/[ZrO_2/AO-MWCNTs-700Ar] in (c) has high current density even after 180 cycles. For Pd/[ZrO_2/AO-MWCNTs-900Ar] and Pd/[ZrO_2/AO-MWCNTs-300Air-900Ar], in (d) and (e), the latter has lower oxidation potential. In (f), Pd/[Pd:ZrO_2/AO-MWCNTs-300Air-900Ar] initially has good current density, but it decays fast.

In order to analyze the behavior of the Pd catalysts in CV test, the maximum current density and the corresponding potential of every 10 cycles were replotted in **Figure 5(a)** and **Figure 5(b)**, respectively. The (a) plot shows the three tetragonal zirconia modified Pd catalysts (red, blue and pink) have the best current density than the others. It is similar to the ECSA results. In (b), Pd/AO-MWCNTs has low potentials 0.3 V in the first 60 cycles, then it changes to higher potential about 0.45 V. It shows Pd/AO-MWCNT conducts a formic acid direct oxidation initially. Pd/[ZrO_2/AO-MWCNTs-700Ar] and Pd/[ZrO_2/AO-MWCNTs-900Ar] have higher but stable corresponding potential about 0.6 V and 0.5 V. Pd/[ZrO_2/AO-MWCNTs-300Air-900Ar has corresponding potential about 0.45 V before 130 cycles then high potential about 0.7 V. The higher temperature treatment of zirconia may decrease the oxidation potential of formic acid. For the tetragonal zirconia modified Pd catalysts, their relative higher corresponding potential indicates formic acid undergoing an indirect path. The produced CO intermediatein the indirect path may be oxidized by tetragonal zirconia. It promises the slower decay in current density of the Pd catalysts. The green curve

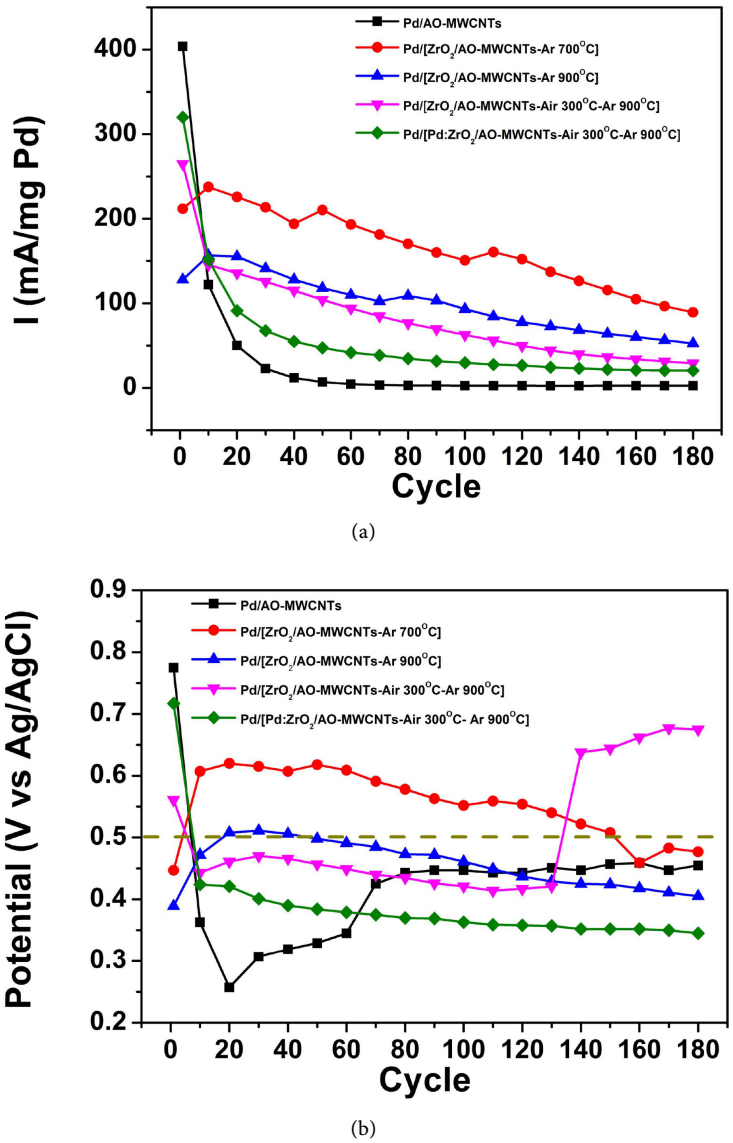

Figure 5. CV analysis: (a) the maximum current density vs cycle, (b) the corresponding potential vs cycle.

of Pd/[Pd:ZrO_2/AO-MWCNTs-300Air-900Ar], with monoclinic and tetragonal zirconia modification, can be recognized as Pd direct oxidation behavior for the potential about 0.35 V. While the aggregation of Pd nanoparticles offsets most zirconia effect in CV test.

The two Pd catalysts, Pd/AO-MWCNTs and Pd/[ZrO_2/AO-MWCNTs(C)-300Air-900Ar], were compared their 60-cycle CV performance of not poisoned and CO poisoned. In **Figure 6**, the poisoned Pd/AO-MWCNTs catalyst (b) decays faster than not poisoned (a). For Pd/[ZrO_2/AO-MWCNTs(C)-300Air-900Ar] in (c) and (d), the 10^{th} cycle maximum current densities are 145.5 mA/mgPd (not poisoned) > 82.4 mA/mgPd (CO poisoned). While for the poisoned Pd/[ZrO_2/AO-MWCNTs(C)-300Air-900Ar], the maximum current density of the 30^{th} and 40^{th} cycles are larger than 150

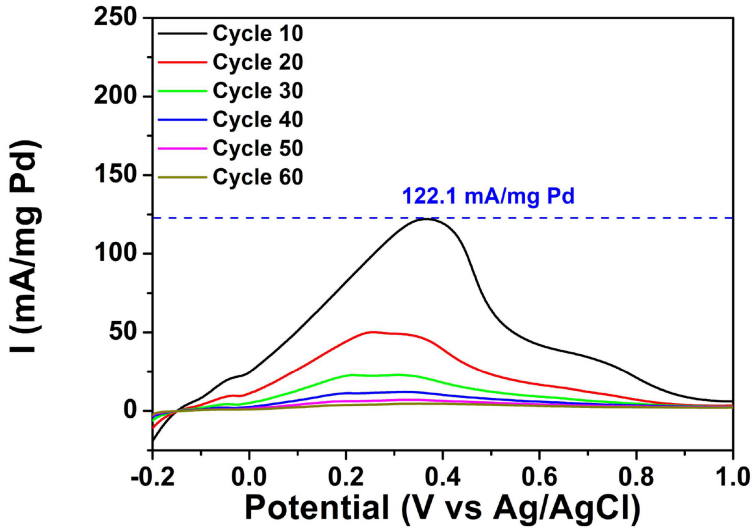
Cycle 10
Cycle 20
Cycle 30
Cycle 40
Cycle 50
Cycle 60
122.1 mA/mg Pd
I (mA/mg Pd)
Potential (V vs Ag/AgCl)

(a)

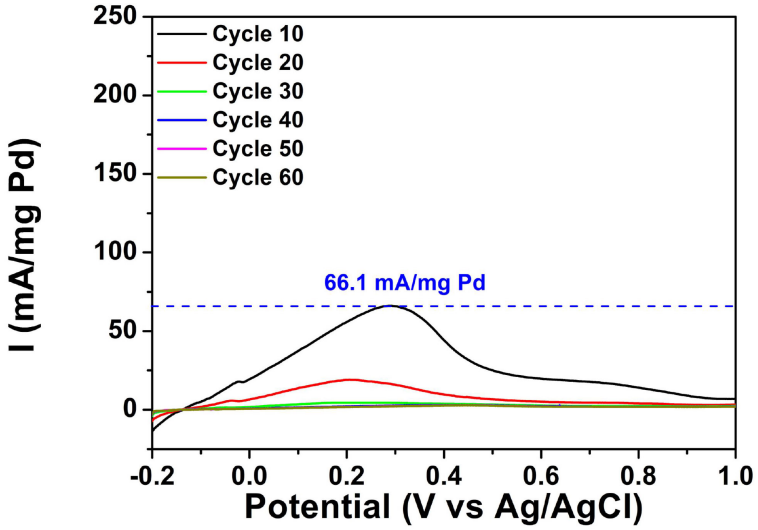
Cycle 10
Cycle 20
Cycle 30
Cycle 40
Cycle 50
Cycle 60
66.1 mA/mg Pd
I (mA/mg Pd)
Potential (V vs Ag/AgCl)

(b)

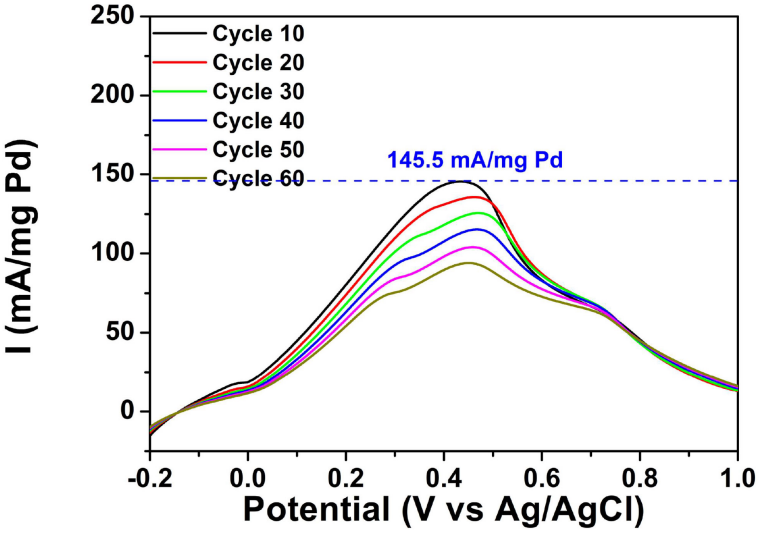
Cycle 10
Cycle 20
Cycle 30
Cycle 40
Cycle 50
Cycle 60
145.5 mA/mg Pd
I (mA/mg Pd)
Potential (V vs Ag/AgCl)

(c)

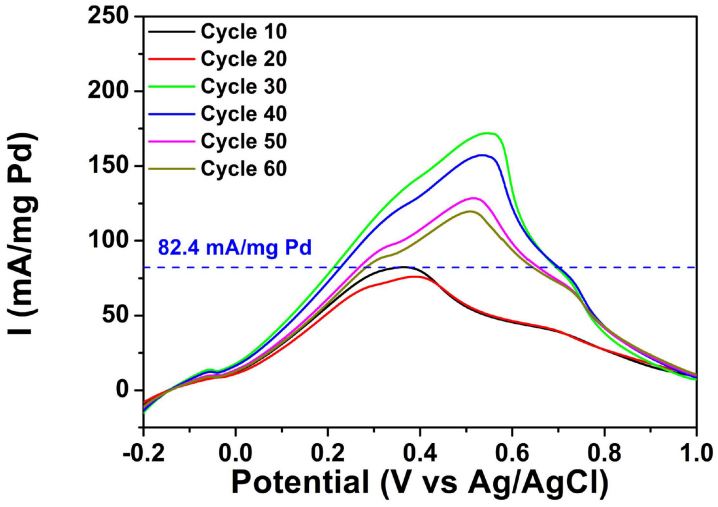

(d)

Figure 6. 60-cycle CV results of (a) Pd/AO-MWCNTs, (b) CO poisoned Pd/AO-MWCNTs, (c) Pd/[ZrO_2/AO-MWCNTs(C)-300Air-900Ar], and (d) CO poisoned Pd/[ZrO_2/AO-MWCNTs(C)-300Air-900Ar].

mA/mgPd. The Pd/[ZrO_2/AO-MWCNTs(C)-300Air-900Ar] seems to be activated by CO reduction and the potential shift to higher voltage. As more cycles, the catalyst still decay due to CO poison. The result reveals the addition of ZrO_2 can improve the resistance of CO poison.

Figure 7 shows the current-time (I-t) behavior of the Pd catalysts in formic acid and sulfuric acid under constant potential of 0.3 V. Pd/[ZrO_2/AO-MWCNTs-300Air-900Ar] and Pd/[Pd:ZrO_2/AO-MWCNTs-300Air-900Ar] are the two best. The two catalysts have the relatively lower and stable corresponding potential in CV indicating direct dehydrogenation path of formic acid. If the catalysts undergo a direct oxidation of formic acid, it will be more stable. Though Pd/[ZrO_2/AO-MWCNTs-700Ar] and Pd/[ZrO_2/AO-MWCNTs-900Ar] have tetragonal zirconia to prevent CO poison, their higher potential formic acid oxidation may not benefit this 0.3 V I-t test.

4. Conclusion

This study prepared different $ZrO_2$by adjusting preparation parameters: carbon nanotubes, 1% Pd adding, sintering temperature and atmospheres. The prepared zirconias are: pure ZrO_2 (tetragonal + monoclinic), ZrO_2/AO-MWCNTs (tetragonal) and Pd:ZrO_2/AO-MWCNTs (tetragonal + monoclinic). The synthesized Pd has more aggregation on the surfaces of Pd:ZrO_2/AO-MWCNTs. The effect of different zirconia for Pd electrocatalytic performance is studied via the CV tests. Tetragonal zirconia modified Pd/ZrO_2/AO-MWCNTs have larger ECSA area values than those others. The more electrochemical active surface may promise better performance in electrocatalytic performance. Through the analysis of maximum current density and the corresponding potential of the

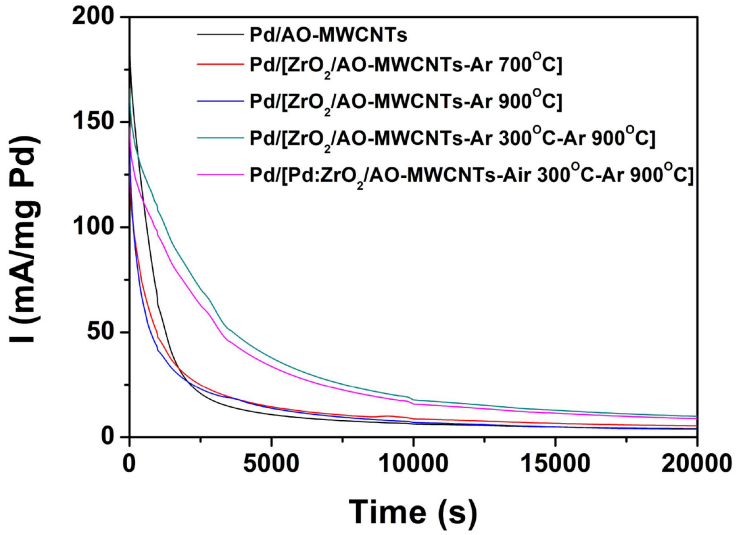

Figure 7. Chronoamperometric measurements (I-t) of the prepared catalysts in 3M HCOOH and 1M H_2SO_4, 0.3 V.

prepared Pd catalysts catalyzed formic acid, Pd/AO-MWCNTs undergo the direct oxidation (lower potential) initially and change to indirect path for CO poisoning Pd. For those three Pd catalysts modified by tetragonal ZrO_2, they have higher current density and higher oxidation potential. It reveals that though the catalysts oxidize formic acid in the indirect path, tetragonal zirconia may release oxygen easier to benefit the CO oxidation and enhance the Pd activity. For Pd/[Pd:ZrO_2/AO-MWCNTs-300Air-900Ar] with tetragonal and monoclinic ZrO_2 modified, monoclinic ZrO_2 may keep more CO than Pd does, and the oxygen deficient monoclinic ZrO_2 may have pseudo metal behavior that helps Pd obtains electron supply as Pd catalyzes formic acid. These cause the lower potential for monoclinic zirconia modified Pd catalysts. In constant potential 0.3 V I-t test, Pd/[ZrO_2/AO-MWCNTs-300Air-900Ar] and Pd/[Pd:ZrO_2/AO-MWCNTs-300Air-900Ar] are the two best catalysts. The former, Pd/[ZrO_2/AO-MWCNTs-300Air-900Ar] with tetragonal zirconia, and the latter, Pd/[Pd:ZrO_2/AO-MWCNTs-300Air-900Ar] with monoclinic zirconia, both directly oxidize formic acid in a lower potential. The two prepared Pd catalysts can be candidates for anodic catalysts in DFAFCs.

Acknowledgements

The authors gratefully acknowledge for the years grants from Taiwan Ministry of Science and Technology (MOST 108-2923-E-036-002-MY3, MOST 106-2221-E-036-021) and Tatung University (B108-C04-011) for financially supporting for this work.

Conflicts of Interest

The authors declare no conflicts of interest regarding the publication of this paper.

References

[1] Yu, X. and Pickup, P.G. (2008) Recent Advances in Direct Formic Acid Fuel Cells (DFAFC). *Journal of Power Sources*, **182**, 124-132. https://doi.org/10.1016/j.jpowsour.2008.03.075

[2] Rice, C.A. and Wieckowski, A. (2013) Electrocatalysis of Formic Acid Oxidation. In: *Electrocatalysis in Fuel Cells*, Platinum, New York, 43-67. https://doi.org/10.1007/978-1-4471-4911-8_3

[3] Marinšek, M., Šala, M. and Jančar, B. (2013) A Study towards Superior Carbon Nanotubes-Supported Pd-Based Catalysts for Formic Acid Electro-Oxidation: Preparation, Properties and Characterisation. *Journal of Power Sources*, **235**, 111-116. https://doi.org/10.1016/j.jpowsour.2013.02.020

[4] Saleem, J., Hossain, S.K.S., Al-Ahmed, A., Rahman, A., McKay, G. and Hossain, M.M. (2018) Evaluation of Pd Nanoparticle-Decorated CeO_2-MWCNT Nanocomposite as an Electrocatalyst for Formic Acid Fuel Cells. *Journal of Electronic Materials*, **47**, 2277-2289. https://doi.org/10.1007/s11664-017-6051-2

[5] Zhou, W. and Lee, J.Y. (2007) Highly Active Core-Shell Au@Pd Catalyst for Formic Acid Electrooxidation. *Electrochemistry Communications*, **9**, 1725-1729. https://doi.org/10.1016/j.elecom.2007.03.016

[6] Yang, S., Zhang, X., Mi, H. and Ye, X. (2008) Pd Nanoparticles Supported on Functionalized Multi-Walled Carbon Nanotubes (MWCNTs) and Electrooxidation for Formic Acid. *Journal of Power Sources*, **175**, 26-32. https://doi.org/10.1016/j.jpowsour.2007.09.080

[7] Li, H., Zhang, Y., Wan, Q., Li, Y. and Yang, N. (2018) Expanded Graphite and Carbon Nanotube Supported Palladium Nanoparticles for Electrocatalytic Oxidation of Liquid Fuels. *Carbon*, **131**, 111-119. https://doi.org/10.1016/j.carbon.2018.01.093

[8] Mazurkiewicz-Pawlicka M., Malolepszy, A., Mikolajczuk-Zychora, A., Mierzwa, B., Borodzinski, A. and Stobinski, L. (2019) A Simple Method for Enhancing the Catalytic Activity of Pd Deposited on Carbon Nanotubes Used in Direct Formic Acid Fuel Cells. *Applied Surface Science*, **476**, 806-814. https://doi.org/10.1016/j.apsusc.2019.01.114

[9] Caglar, A., Ulas, B., Cogenli, M.S., Yurtcan, A.B. and Kivrak, H. (2019) Synthesis and Characterization of Co, Zn, Mn, V Modified Pd Formic Acid Fuel Cell Anode Catalysts. *Journal of Electroanalytical Chemistry*, **850**, 113402. https://doi.org/10.1016/j.jelechem.2019.113402

[10] Chiou, Y.J., Chung, M.Y., Lin, H.M., Liu, H.Y., Borodzinski, A., Stobinski, L., Lin, C.K. and Kupiec, K.R. (2017) Synthesis and Characterization of PANI-MWCNTs Supported Nano Hybrid Electrocatalysts. *Journal of Materials Science and Engineering A*, **7**, 1-8. https://doi.org/10.17265/2161-6213/2017.1-2.001

[11] Chiou, Y.J., Chen, K.Y., Lin, H.M., Liou, W.J., Liou, H.W., Wu, S.H., Mikolajczuk, A., Mazurkiewicz, M., Malolepszy, A., Stobinski, L., Borodzinski, A., Kedzierzawski, P., Kurzydlowski, K., Chien, S.H. and Chen, W.C. (2011) Electrocatalytic Properties of Hybrid Palladium-Gold/Multi-Walled Carbon Nanotube Materials in Fuel Cell Applications. *Physical Status Solidi A*, **208**, 1778-1782. https://doi.org/10.1002/pssa.201001213

[12] Lee, Y.L., Chiou, Y.J. and Lin, H.M. (2015)The Synthesis and Characterization of Nano Noble Metals/WO_3/MWCNTs Hybrid Electrocatalysts. *Tatung Journal*, **30**, 27-32.

[13] Kung, H.M., Chiou, Y.J., Lin, H.M., Borodzinski, A., Stobinski, L. and Lin, C.K.

(2016) Anode Catalyst of Hybrid AuPd and Rare Earth Doped Cerium Oxide/Multi-Walled Carbon Nanotubes for Direct Formic Acid Fuel Cells. *Journal of the Japan Society of Powder and Powder Metallurgy*, **63**, 706-713. https://doi.org/10.2497/jjspm.63.706

[14] Chiou, Y.J., Lu, C.D., Lin, H.M., Borodzinski, A., Stobinski, L. and Lin, C.K. (2015) Synthesis and Characterization of Nano-Hybrid Noble Metals/N Doped TiO_2/MWCNTs Electrocatalysts. *International Journal of Chemical Engineering*, **2**, 68-72.

[15] Terki, R., Bertrand, G., Aourag, H. and Coddet, C. (2006) Structural and Electronic Properties of Zirconia Phases: A FP-LAPW Investigations. *Materials Science in Semiconductor Processing*, **9**, 1006-1013. https://doi.org/10.1016/j.mssp.2006.10.033

[16] Bouvier, P., Djurado, E., Lucazeau, G. and Le Bihan, T. (2000) High-Pressure Structural Evolution of Undoped Tetragonal Nanocrystalline Zirconia. *Physical Review B*, **62**, 8731. https://doi.org/10.1103/PhysRevB.62.8731

[17] Prakasam, M., Valsan, S., Lu, Y., Balima, F., Lu, W., Piticescu, R. and Largeteau, A. (2018) Nanostructured Pure and Doped Zirconia: Synthesis and Sintering for SOFC and Optical Applications. Sintering Technology: Method and Application. https://doi.org/10.5772/intechopen.81323

[18] Lesiak, B., Malolepszy, A., Mazurkiewicz-Pawlicka, M., Stobinski, L., Kövér, L., Tóth, J., Mierzwa, B. and Trykowski, G. (2018) A High Stability AuPd-ZrO_2-Multiwall Carbon Nanotubes Supported-Catalyst in a Formic Acid Electro-Oxidation Reaction. *Applied Surface Science*, **451**, 289-297. https://doi.org/10.1016/j.apsusc.2018.04.233

[19] Sinhamahapatra, A., Jeon, J.P., Kang, J., Han, B. and Yu, J.S. (2016) Oxygen-Deficient Zirconia (ZrO_{2-x}): A New Material for Solar Light Absorption. *Scientific Reports*, **6**, 27218. https://doi.org/10.1038/srep27218

[20] Kouva, S., Honkala, K., Lefferts, L. and Kanervo, J. (2015) Review: Monoclinic Zirconia, Its Surface Sites and Their Interaction with Carbon Monoxide. *Catalysis Science & Technology*, **5**, 3473-3490. https://doi.org/10.1039/C5CY00330J

Scientific Research Publishing

Advances in Chemical Engineering and Science, 2020, 10, 113-122
https://www.scirp.org/journal/aces
ISSN Online: 2160-0406
ISSN Print: 2160-0392

Methanation of Syngas over Ni-Based Catalysts with Different Supports

Buyan-Ulzii Battulga, Munkhdelger Chuluunsukh, Enkhsaruul Byambajav

Laboratory of Clean Energy Technology Development, School of Arts & Sciences, National University of Mongolia, Ulaanbaatar, Mongolia
Email: battulgabuyanaa@gmail.com

How to cite this paper: Battulga, B.-U., Chuluunsukh, M. and Byambajav, E. (2020) Methanation of Syngas over Ni-Based Catalysts with Different Supports. *Advances in Chemical Engineering and Science*, **10**, 113-122.
https://doi.org/10.4236/aces.2020.102008

Received: March 18, 2020
Accepted: April 25, 2020
Published: April 28, 2020

Abstract

CO methanation over the 20% nickel catalyst prepared by impregnation-precipitation method on different supports of commercial γ-Al_2O_3, TiO_2, SiO_2 and nano-γ-Al_2O_3* was investigated. The nano-γ-Al_2O_3* support was pulverized using a ball milling method. Catalyst characterization was done using the methods of BET, XRD, SEM, ICP-OES methods. Carbon monoxide methanation process was carried out at the temperature of 350˚C in pressure of 3 bar of H_2:CO syngas with the molar ratio of 3:1 and with the GHSV of 3000 h^{-1} in a fixed bed reactor. The initial temperature of methane formation increased according to the order of Ni/γ-Al_2O_3* < Ni/SiO_2 < Ni/γ-TiO_2 < Ni/γ-Al_2O_3. The Ni/γ-Al_2O_3*, which was prepared on the surface of nano milled γ-Al_2O_3 support, produced methane from the lowest temperature of 178˚C to 350˚C in CO methanation. The Ni/γ-Al_2O_3* catalyst gave the highest amount of methane (0.1224 mmol/g-cat) for 1 h methanation among other catalysts. XRD and SEM analysis proved that NiO particles in the Ni/γ-Al_2O_3* were finely distributed, and their sizes were smaller compared to those in the traditional one. The pulverization of γ-Al_2O_3 improved the dispersion of catalytic active nickel species inside porosity of the support leading to the improvement of its catalytic performance for CO methanation.

Keywords

CO Hydrogenation, Water-Gas Shift Reaction, Nano-γ-Al_2O_3, Methane Productivity

1. Introduction

Synthetic natural gas (SNG) as a clean energy carrier has been attracted increasing attention worldwide owing to its lower emissions of sulfur, nitrogen and dust

than that of direct using coal and is expected to be one of the main energy sources in the 21st century [1]. This process mainly includes coal gasification to syngas and methanation of syngas, in which methanation is a critical step with the reactions as shown in Equation (1) and Equation (2) [2].

$$CO + 3H_2 \rightarrow CH_4 + H_2O \ \Delta H = -206 \text{ kJ/mol} \quad (1)$$

$$CO_2 + 4H_2 \rightarrow CH_4 + 2H_2O \ \Delta H = -165 \text{ kJ/mol} \quad (2)$$

Rhodium, ruthenium and nickel are known to be catalytically active for CO and CO_2 methanation reaction. However, nickel is estimated as the most suitable commercial catalyst because of its reasonable cost and high selectivity [3] [4] [5]. The activity of Ni based catalyst can be affected by support types, preparation methods and promoters [6]-[13]. MgO, Al_2O_3, SiO_2, TiO_2 and ZrO_2 are used as a catalyst support for Ni catalyst in methanation; and these supports can affect the activities of methanation catalyst through changing the particles size and distribution of Ni active component [6]. Takenaka *et al.* [10] reported that the activity of supported Ni catalysts for CO methanation was strongly dependent on the type of catalytic supports, and the observed conversions of CO at 526 K were higher in the order of Ni/MgO < Ni/Al_2O_3 < Ni/SiO_2 < Ni/TiO_2 < Ni/ZrO_2 [8]-[14]. Also, Liu *et al.* [15] showed that when the supports of Al_2O_3, CeO_2 and ZrO_2 were tested at low temperature of CO methanation, catalytic activity of Ni increased according to the order of Ni/CeO_2 < Ni/ZrO_2 < Ni/γ-Al_2O_3. The last one presented the best catalytic performance with the highest CH_4 selectivity of 94.5% [15].

In the present study, γ-Al_2O_3, TiO_2, SiO_2 were selected as a catalyst support for nickel in CO methanation. Since it is supposed that catalyst support should be an important factor for the preparation of fine species of Ni active catalysts, we tested a pulverization of γ-Al_2O_3 prior to precipitation of active metal to γ-Al_2O_3 support. This research work described an effect of different supports on nickel distribution and particle size, and also an influence of nano milling of Ni/γ-Al_2O_3 support on catalytic performances for CO methanation.

2. Experimental Method

Pulverization of γ-Al_2O_3 support prior to precipitation of Ni catalyst

Pulverization of γ-Al_2O_3 was carried out using a high energy planetary ball mill described in **Figure 1(a)**, **Figure 1(b)**. A planetary ball mill (HPM-700, Haji Engineering, Korea), as shown in **Figure 1(a)**, was used to grind the samples in this study. Ball milling process is a mechanical process which relies on an energy released at the point of collision between balls as well as on the high grinding energy created by friction of balls on the wall. As shown in **Figure 1(b)**, zirconia balls with 5 mm of diameter were placed in a sintered corundum container. When the mill rotates, balls are picked up by mill wall and rotate around the wall due to centrifugal force leading to grinding of material due to frictional effect. There is also reverse rotation of disc with respect to mill which applies centrifugal force in opposite direction leading to transition of balls on opposite walls

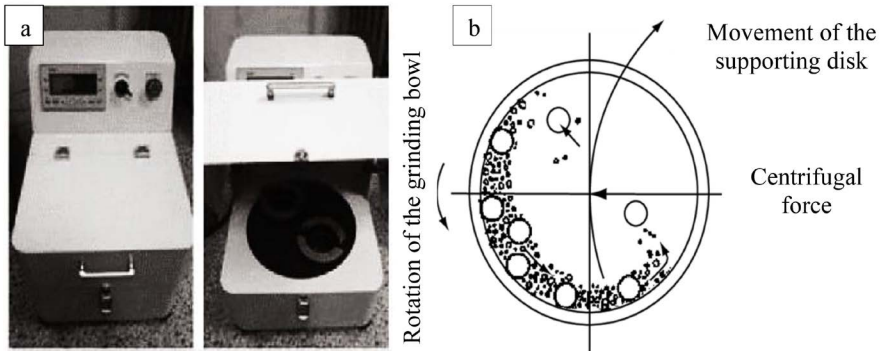

Figure 1. Photo of mill (a) and working principle of ball milling process (b).

of mill. The zirconia ball to sample weight ratio was 10:1. A rotation speed of the planet carrier was 500 rpm. The pulverization of γ-Al_2O_3 was performed for 10 min of dry milling.

Catalyst precipitation method

The different supported Ni catalysts were prepared by impregnation-precipitation method [16] [17] [18]. Initially, catalyst support was dissolved in deionized water of 100 ml. The suspension was heated to 50˚C and maintained at that temperature for 30 min. Amount of 10.11 g of $Ni(NO_3)_2{\cdot}6H_2O$ as a nickel precursor was dissolved in 300 ml of deionized water. A slight excess stoichiometrically of Na_2CO_3 aqueous solution with a volume of 300 ml was added dropwise (pH ≈ 9) to the previous solution for precipitation. After stirring continuously for another 1 h at 50˚C, the carbonate precipitate was removed by filtration, then it is washed by deionized water three times. Then, the precipitate was dried overnight at 110˚C, followed by heating to 500˚C with a ramp rate of 2˚C/min for calcination in air for 4 h. The catalysts were denoted as Ni/γ-Al_2O_3, Ni/γ-Al_2O_3* (nano), Ni/TiO_2, Ni/SiO_2. All catalysts were pressed into pellets, and then they were further crushed into particles of 45 - 90 mesh, and their activities were evaluated in CO methanation.

Evaluation of catalyst performance

Catalytic test for CO methanation was carried out in a stainless steel tubular reactor with the inner diameter of 8 mm. About 1 g catalyst was used for each test. Catalysts were activated in a hydrogen flow of 13 ml/min at 400˚C with a heating rate of 5˚C/min for 2 h. After activation, a feed syngas with a volume ratio of $3H_2$:1CO was introduced to the reactor, and its flow rate was controlled by an MFC. Methanation was performed at pressure of 3 bar and with a GHSV of 3000 h^{-1} in the temperature of 350˚C. Gas products were separated through a cooler, and analyzed online by a gas chromatography (GC; YL-6100) with a thermal conductivity detector (TCD). The CO conversion, CH_4 yield and selectivity were calculated using the following Equations (3)-(5), respectively.

CO conversion:

$$X_{CO}(\%) = \frac{V_{CO,inlet} - V_{CO,outlet}}{V_{CO,inlet}} \times 100 \quad (3)$$

Methane selectivity:

$$S_{CH_4}(\%) = \frac{V_{CH_4,outlet}}{V_{CH_4,outlet} + V_{CO_2,outlet} + V_{H_2,outlet}} \times 100 \quad (4)$$

Methane yield:

$$Y_{CH_4}(\%) = \frac{X_{CO} \times S_{CH_4}}{100} \quad (5)$$

Catalyst characterizations

BET surface area was measured by nitrogen adsorption at the liquid nitrogen temperature on a Flowsorb III 2305/2310 analyzer. Prior to analysis, the samples were degassed under dynamic vacuum at 150˚C for 30 min.

XRD measurement was carried out on a mini Flex 600 diffractometer with a monochromatic Co Kα radiations source (λ = 1.7903). The scans were performed from 5˚ to 95˚ of 2θ angle with a step size of 0.02˚.

Nickel contents in fresh catalysts were determined using by 6500 ICP-OES analyzer.

SEM images were obtained on the JEOL JSM 7001F microscope operated at 10 - 20 kV. The sample was fixed on a carbon black holder with conductive adhesives.

3. Results and Discussion

After the impregnation-precipitation, actual contents of nickel catalysts were measured using a method of ICP-OES. Table 1 shows the nominal and experimental contents of nickel metal precipitated on the different supports by the impregnation-precipitation method.

It was identified that when nickel content of the catalysts was nominally expected as 20 wt%, the obtained contents were between in approximately 17 - 18 wt% depending on different supported catalysts.

Catalyst activity of the Ni/γ-Al_2O_3* catalyst was compared with those of Ni/γ-Al_2O_3, Ni/TiO_2 and Ni/SiO_2 in Figure 2. Activities of the obtained catalysts prepared on different supports were examined at the reaction temperature of 350˚C under the syngas pressure of 3 bar.

It was found that Ni/SiO_2 catalyst gave the best activity at the equilibration temperature of 350˚C, and the CH_4 yield reached 85.7%. However, the nano-Ni/γ-Al_2O_3* catalyst produced a methane from the lowest temperature fitted around 35 minutes of time on stream. This catalyst gave the CH_4 yield of 78.7% at the equilibration temperature of 350˚C. As shown in Figure 2, the activity of Ni/TiO_2 was similar to that of Ni/γ-Al_2O_3.

Table 2 compared the methane yield and the initial temperature of its formation. The initial temperature of methane formation increased according to the order of Ni/γ-Al_2O_3* < Ni/SiO_2 < Ni/γ-TiO_2 < Ni/γ-Al_2O_3. The Ni/γ-Al_2O_3* produced methane from the lowest temperature of 178˚C to 350˚C in CO methanation.

Table 1. Nickel contents after precipitation on the different supports by an impregnation-precipitation method.

Catalyst code	Support	Ni content, (wt %)	
		Nominal	Experimental[1)]
Ni/γ-Al_2O_3	γ-Al_2O_3	20	17
Ni/γ-Al_2O_3* (nano)	γ-Al_2O_3	20	18
Ni/TiO_2	TiO_2	20	17
Ni/SiO_2	SiO_2	20	18

[1)]Determined by ICP-OES analysis.

Table 2. Comparison of CO methanation performance for Ni/γ-Al_2O_3, Ni/γ-Al_2O_3*, Ni/TiO_2 and Ni/SiO_2 catalysts.

Catalyst code	CH_4 yield, %	Initial temperature of CH_4 formation, ˚C
Ni/γ-Al_2O_3	75.4	268
Ni/γ-Al_2O_3* (nano)	78.7	178
Ni/TiO_2	80.4	250
Ni/SiO_2	85.7	218

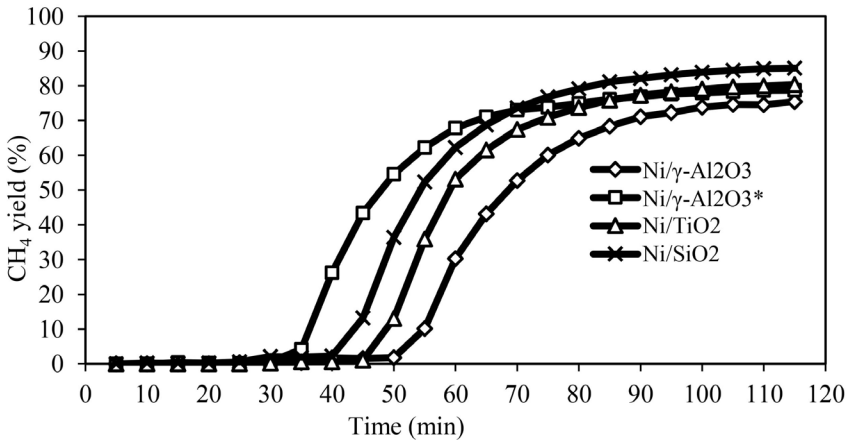

Figure 2. Methane yield obtained during synthesis with the catalysts prepared on different supports.

Activity of Ni/γ-Al_2O_3* prepared with support pulverization was higher than that of traditional Ni/γ-Al_2O_3, and the CH_4 yield reached 78.7%.

Figure 3 shows that the Ni/γ-Al_2O_3* catalyst converts almost fully the carbon monoxide into methane. In the end of reaction, the content of CO was only 0.62 % in product gas.

With decreasing the CO content in a feed gas, the methane yield is increasing sharply from 30 minutes to 60 minutes of time on stream, then it was slowly increasing at the equilibration temperature of 350˚C. Regarding temperature program, methanation temperature reaches the equilibration temperature around 60 minutes of time on stream.

Figure 4 shows the CH_4 productivities, which were calculated by a sum of

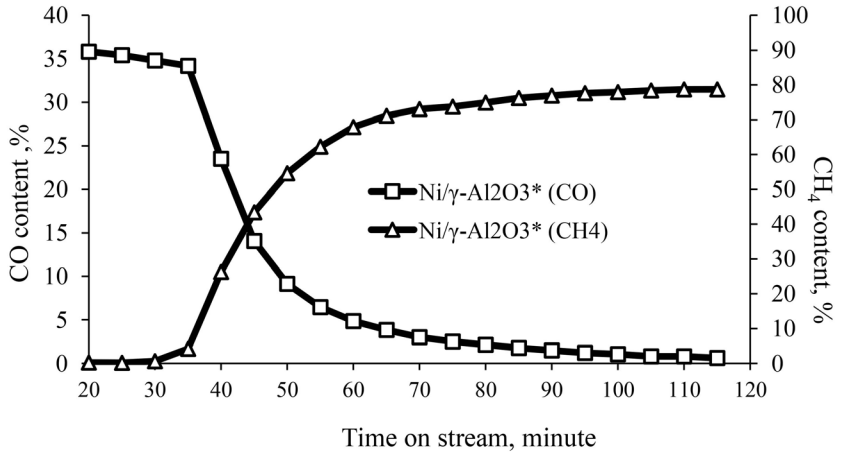

Figure 3. CO and CH_4 contents during methanation synthesis with the Ni/γ-Al_2O_3*.

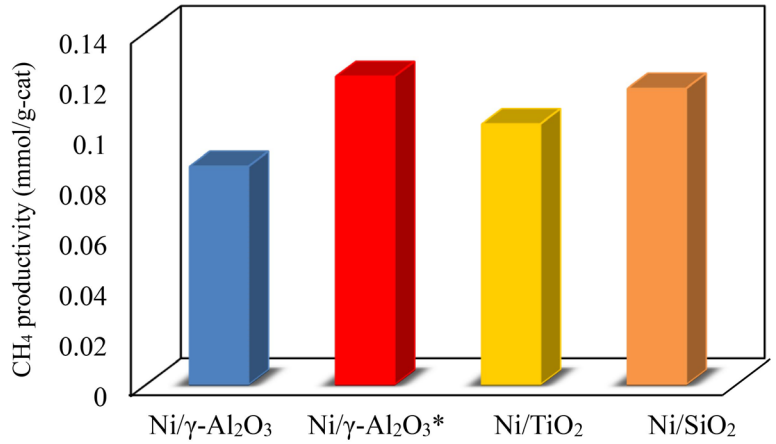

Figure 4. CH_4 productivities of Ni/γ-Al_2O_3, Ni/γ-Al_2O_3*, Ni/TiO_2 and Ni/SiO_2 catalysts in CO methanation at 350˚C.

produced CH_4 amount per unit of catalyst weight for 1 h methanation, with the Ni/γ-Al_2O_3, Ni/γ-Al_2O_3*, Ni/TiO_2 and Ni/SiO_2 catalysts in CO methanation at 350˚C. It was known that the Ni/γ-Al_2O_3* catalyst produced the highest amount of methane (0.1224 mmol/g-cat) for 1 h methanation among the four catalysts. However, the traditional Ni/γ-Al_2O_3 catalyst gave the lowest amount of methane (0.0867 mmol/g-cat) for 1 h methanation, although it contains the same amount of nickel catalyst as that in the Ni/γ-Al_2O_3* catalyst prepared using the nano milled γ-Al_2O_3 support. The structures of the two compared catalysts were further analyzed by SEM and XRD analysis.

The SEM images of Ni/γ-Al_2O_3 and Ni/γ-Al_2O_3* catalysts are shown in **Figure 5(a)** and **Figure 5(b)**. As shown in **Figure 5(a)**, there were large crevices and cracks, which were illustrated by dark part of SEM image, on the surface of Ni/γ-Al_2O_3. However, **Figure 5(b)** shows a uniform porous structure illustrated by bright part for metal oxides in the SEM without any large cracks and crevices. It suggests a formation of fine Ni nanoparticles distributed on the surface of nano milled γ-Al_2O_3* support. The porous structure of the last support provided

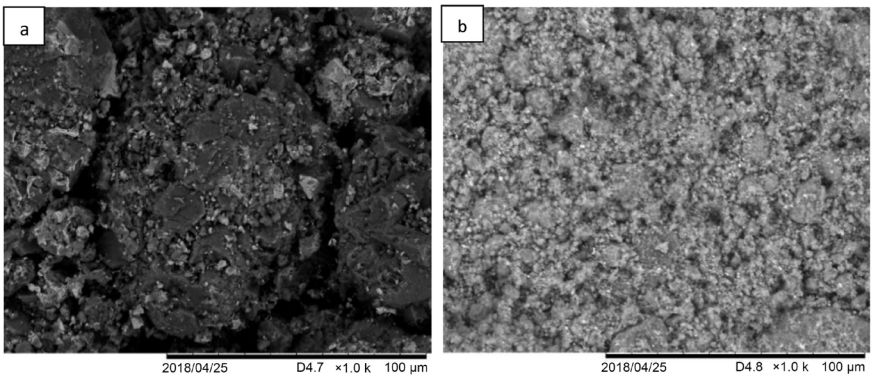

Figure 5. SEM images of the fresh catalysts: (a) Ni/γ-Al_2O_3 and (b) Ni/γ-Al_2O_3*.

the good dispersion of active nickel catalyst leading to high activity and selectivity for methane. Figure 6 describes the X-ray diffractograms of the fresh catalysts of Ni/γ-Al_2O_3, Ni/γ-Al_2O_3*, Ni/TiO_2 and Ni/SiO_2 before methanation process.

The characteristic diffraction peaks of γ-Al_2O_3 support and NiO appear at 53.55˚ and 79.59˚; and at 43.45˚, 50.63˚ and 74.43˚, respectively for the fresh catalysts [16] [17] [18]. For all catalysts prepared by the impregnation-precipitation method, no nickel aluminate species, which were inactive catalytically and non-reducible ones formed by strong interactions between nickel particles and catalyst support, were created in the catalysts. For the Ni/SiO_2 catalyst, two broad diffraction peaks in 2θ region of 15.5˚ - 30.0˚ were attributed to the diffraction characteristics of amorphous SiO_2. For the Ni/TiO_2 catalyst, the peaks in 2θ region of 25.3˚, 43.8˚, 55.0˚ were attributed to the anatase phase of TiO_2. The particle sizes were calculated from the Scherrer formula (6) based on the peak width at 50.63˚ reflection. The results are listed in Table 3. Intensity of the peak at 50.63˚ of NiO species in Ni/γ-Al_2O_3 was the strongest among other catalysts, even though their nickel contents were similar (see Figure 7). Its NiO particle size calculated by the Scherrer equation was the largest of 21 nm among other catalysts. Moreover, Table 3 shows the smaller particles of nickel oxides in Ni/γ-Al_2O_3*, Ni/TiO_2 and Ni/SiO_2 catalysts.

$$\tau = \frac{K * \lambda}{\beta * \cos\theta} \tag{6}$$

τ—Particle size

K— Shape factor

λ— X-ray wavelength

β—half the maximum intensity (FWHM)

θ—Bragg angle

For the Ni/γ-Al_2O_3* and the Ni/γ-Al_2O_3 catalysts, a surface area of catalyst was smaller for the catalyst prepared on the nano milled support of γ-Al_2O_3. It might be suggested that more fine particles of NiO species filled inside porous structure of the nano milled support.

Figure 8 shows the X-ray diffractograms of the used Ni/γ-Al_2O_3, Ni/γ-Al_2O_3*,

Table 3. BET surface area and NiO particle size of the fresh catalysts of Ni/γ-Al_2O_3, Ni/γ-Al_2O_3*, Ni/TiO_2 and Ni/SiO_2.

Catalyst code	S_{BET} (m^2/g)	NiO particle size[1)] (nm)
Ni/γ-Al_2O_3	131	21
Ni/γ-Al_2O_3* (nano)	115	5
Ni/TiO_2	23.1	14
Ni/SiO_2	110	<5

[1)]Calculated from the peak width at 50.63˚ using Scherrer equation from XRD.

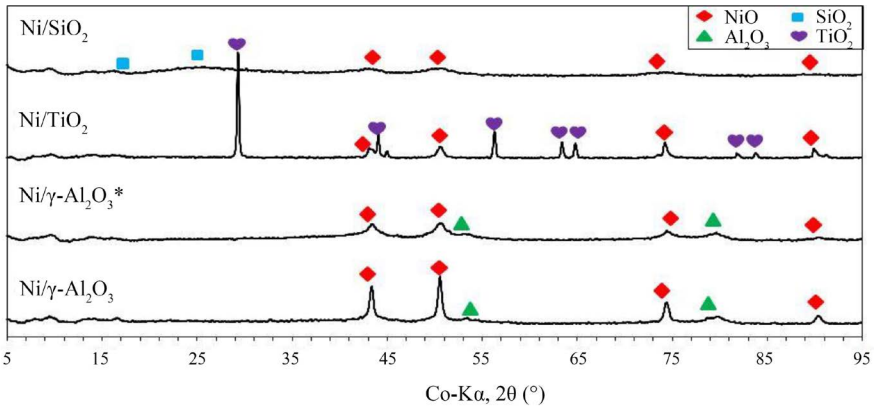

Figure 6. X-ray diffractograms of the obtained catalysts of Ni/γ-Al_2O_3, Ni/γ-Al_2O_3*, Ni/TiO_2 and Ni/SiO_2.

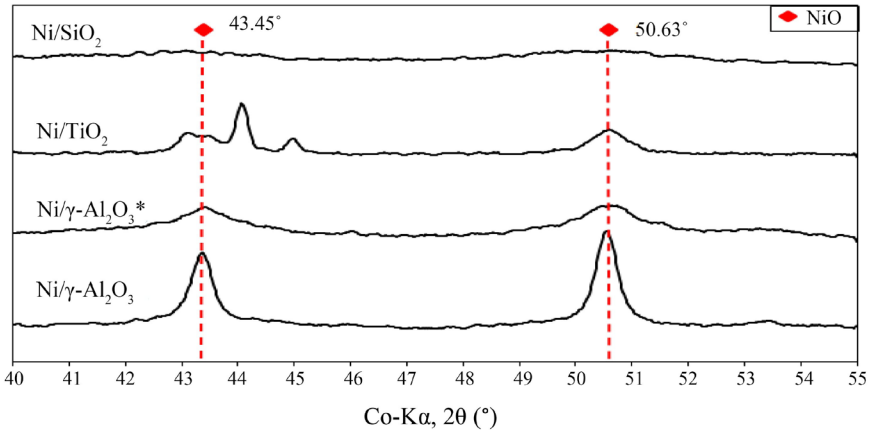

Figure 7. X-ray diffractograms of NiO particles in the Ni/γ-Al_2O_3, Ni/γ-Al_2O_3*, Ni/TiO_2 and Ni/SiO_2.

Ni/TiO_2 and Ni/SiO_2 catalysts after methanation for 1h at 350˚C. It was known that NiO particles were converted to metal Ni (peaked around at 50.6˚ and 60.9˚) by hydrogen activation for all catalysts, and there were no compounds of nickel catalysts formed due to catalyst deactivation caused by interaction between metal and support during activation and methanation. As shown in Figure 8, it was also identified that crystallinity of metallic Ni was very sharp for only the Ni/γ-Al_2O_3. It might depend on easy agglomeration of large nickel particles in the Ni/γ-Al_2O_3 in the present reaction conditions.

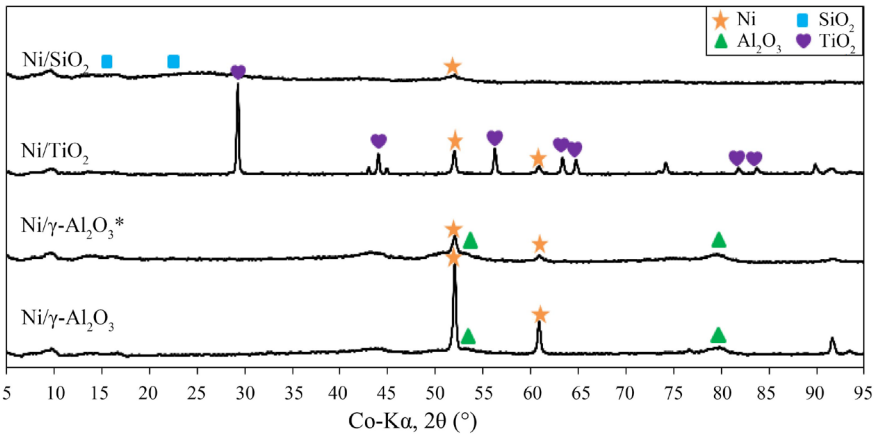

Figure 8. X-ray diffractograms of the used Ni/γ-Al_2O_3, Ni/γ-Al_2O_3*, Ni/TiO_2 and Ni/SiO_2 catalysts after methanation for 1 h.

It is noticeable that the metallic Ni peak at 50.6˚ of Ni/γ-Al_2O_3* catalyst is smaller than Ni/γ-Al_2O_3, implying that the pulverization of γ-Al_2O_3 improved the dispersion of traditional Ni/γ-Al_2O_3 catalyst.

4. Conclusions

1) The initial temperature of methane formation increased according to the order of Ni/γ-Al_2O_3* < Ni/SiO_2 < Ni/γ-TiO_2 < Ni/γ-Al_2O_3. The Ni/γ-Al_2O_3*, which was prepared on the surface of nano milled γ-Al_2O_3 support, produced methane from the lowest temperature of 178˚C to 350˚C in CO methanation.

2) The Ni/γ-Al_2O_3* catalyst gave the highest amount of methane (0.1224 mmol/g-cat) for 1 h methanation among other catalysts of the traditional Ni/γ-Al_2O_3, Ni/SiO_2 and Ni/γ-TiO_2.

3) XRD and SEM analysis proved that NiO particles in the Ni/γ-Al_2O_3* were finely distributed, and their sizes were smaller compared to those in the traditional one. The pulverization of γ-Al_2O_3 improved the dispersion of catalytic active nickel species inside porosity of the support leading to the improvement of its catalytic performance.

Conflicts of Interest

The authors declare no conflicts of interest regarding the publication of this paper.

References

[1] Ronsch, S. (2016) Review on Methanation: From Fundamentals to Current Projects. *Fuel*, **166**, 276-296. https://doi.org/10.1016/j.fuel.2015.10.111

[2] Kohei, U., Yuta, T., Yuta, N., Ryuji, K. and Shigeo, S. (2013) Effects of Preparation Conditions of Ni/TiO_2 Catalysts for Selective CO Methanation in the Reformate Gas. *Fuel*, **452**, 174-178. https://doi.org/10.1016/j.apcata.2012.06.021

[3] Shen, D. and Cheng, C. (2017) Methanation of Syngas (H_2/CO) over the Difference Ni-Based Catalysts. *Fuel*, **189**, 419-427. https://doi.org/10.1016/j.fuel.2016.10.122

[4] Schilidhauer, T.J. (2010) Production of Synthetic Natural Gas (SNG) from Coal and Dry Biomass: A Technology Review from 1950 to 2009. *Fuel*, **89**, 1763-1783. https://doi.org/10.1016/j.fuel.2010.01.027

[5] Song, I.K. (2012) Hydrogenation of Carbon Monoxide to Methane over Mesoporous Nickel-M-Alumina (M = Fe, Ni, Co, Ce, and La) Xerogel Catalysts. *Journal of Industrial and Engineering Chemistry*, *Fuel*, **18**, 243-248. https://doi.org/10.1016/j.jiec.2011.11.026

[6] Max-Michael, W., *et al.* (2008) Walter Lurgi's Methanation Technology for Production of SNG from Coal. Ulrich Berger Lurgi.

[7] Zhang, J., *et al.* (2014) Low-Temperature Methanation of Syngas in Slurry Phase over Zr-Doped Ni/γ-Al_2O_3 Catalysts Prepared Using Different Methods. *Fuel*, **132**, 211-218. https://doi.org/10.1016/j.fuel.2014.04.085

[8] Baowang, L. and Katsuya, K. (2013) Preparation of the Highly Loaded and Well-Dispersed NiO/SBA-15 for Methanation of Producer Gas. *Fuel*, **103**, 669-704. https://doi.org/10.1016/j.fuel.2012.09.009

[9] Mengdie, C., Jie, W., Wei, C., Xueqing, C. and Li, Z.J. (2011) Methanation of Carbon Dioxide on Ni/ZrO_2-Al_2O_3 Catalysts: Effects of ZrO_2 Promoter and Preparation Method of Novel ZrO_2-Al_2O_3 Carrier. *Fuel*, **20**, 318-324. https://doi.org/10.1016/S1003-9953(10)60187-9

[10] Takenaka, S., Shimizu, T. and Otsuka, K. (2004) Complete Removal of Carbon Monoxide in Hydrogen-Rich Gas Stream through Methanation over Supported Metal Catalysts. *International Journal of Hydrogen Energy*, **29**, 1065-1073. https://doi.org/10.1016/j.ijhydene.2003.10.009

[11] Andrigo, P., Bagatin, R., Pagani, G., *et al.* (1999) Fixed Bed Reactor. *Catalyst Today*, **52**, 197-221. https://doi.org/10.1016/S0920-5861(99)00076-0

[12] Hoekman, S.K. and Broch, A. (2010) CO_2 Recycling by Reaction with Renewably Generated Hydrogen. *International Journal of Greenhouse Gas Control*, **4**, 44-50. https://doi.org/10.1016/j.ijggc.2009.09.012

[13] Mohseni, F. and Magnusson, M. (2012) Biogas from Renewable Electricity: Increasing a Climate Neutral Fuel Supply. *Applied Energy*, **90**, 11-16. https://doi.org/10.1016/j.apenergy.2011.07.024

[14] Barelli, L., Bidini, G., Gallorini, F. and Servili, S. (2008) Hydrogen Production through Sorption-Enhanced Steam Methane Reforming and Membrane Technology: A Review. *Energy*, **33**, 554-570. https://doi.org/10.1016/j.energy.2007.10.018

[15] Liu, Z., Chu, B. and Zhai, X. (2012) Total Methanation of Syngas to Synthetic Natural Gas over Ni Catalyst in a Micro-Channel Reactor. *Fuel*, **9**, 559-605. https://doi.org/10.1016/j.fuel.2011.12.045

[16] Buyan-ulzii, B., Daariimaa, O., Munkhdelger, C., Oyunbileg, G. and Enkhsaruul, B. (2018) Effect of Nickel Precursor and Catalyst Activation Temperature on Methanation Performance. *Mongolian Journal of Chemistry*, **19**, 12-18. https://doi.org/10.5564/mjc.v19i45.1084

[17] Barsbold, K., Buyan-ulzii, B. and Enkhsaruul, B. (2018) Carbon Monoxide Methanation: Effect of Catalyst Preparation Method. *Journal of Mongolian Chemical Society*, **13**, 50-62.

[18] Buyan-ulzii, B., Oyunbileg, G. and Enkhsaruul, B. (2018) Carbon Monoxide Methanation: Effect of Catalyst Preparation Method. *Fossil Fuel Chemistry*, *Processing and Ecology Issue*, *Ulaanbaatar*, **6**, 21-29.

Call for Papers

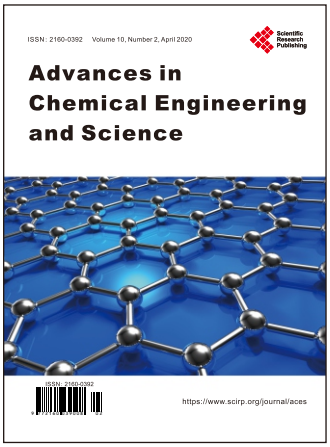

Advances in Chemical Engineering and Science

ISSN: 2160-0392 (Print), 2160-0406 (Online)
https://www.scirp.org/journal/aces

Advances in Chemical Engineering and Science is an open access, peer-reviewed and fully refereed journal focusing on theories, methods and applications in chemical engineering and science. The goal of this journal is to provide a platform for scientists and academicians all over the world to promote, share, and discuss various new issues and developments in different areas of Advances in Chemical Engineering and Science.

Editor-in-Chief

Subject Coverage

All manuscripts must be prepared in English, and are subject to a rigorous and fair peer-review process. Accepted papers will immediately appear online followed by printed hard copy. The journal publishes original papers including but not limited to the following fields:

- Biochemical Engineering
- Bio-Engineering Materials
- Chemical Engineering Biotechnology
- Chemical Reaction
- Chemical Reaction Related Unit Operations
- Chemicals
- Composite Materials
- Electrochemistry of Nanomaterials and Applications
- Energy Engineering
- Environmental Engineering
- Fluid Mechanics
- Green Chemistry
- Molecular Assembly
- Nanomaterials
- Nano-Scale Phenomena
- Nanostructured Materials
- Nanotechnology
- Natural Products
- Optimization of Chemical Engineering Systems
- Organic Chemistry
- Petrochemical
- Pharmaceuticals Polymers
- Specialty Chemicals
- Transport Phenomena

We are also interested in short papers (letters) that clearly address a specific problem, and short survey or position papers that sketch the results or problems on a specific topic. Authors of selected short papers would be invited to write a regular paper on the same topic for future issues of the ***ACES***.

Notes for Intending Authors

Submitted papers should not be previously published nor be currently under consideration for publication elsewhere. Paper submission will be handled electronically through the website. All papers will be peer reviewed. For more derails about the submission, please access the website.

Website and E-Mail

https://www.scirp.org/journal/aces **E-mail: aces@scirp.org**

What is SCIRP?

Scientific Research Publishing (SCIRP) is one of the largest Open Access journal publishers. It is currently publishing more than 200 open access, online, peer-reviewed journals covering a wide range of academic disciplines. SCIRP serves the worldwide academic communities and contributes to the progress and application of science with its publication.

What is Open Access?

All original research papers published by SCIRP are made freely and permanently accessible online immediately upon publication. To be able to provide open access journals, SCIRP defrays operation costs from authors and subscription charges only for its printed version. Open access publishing allows an immediate, worldwide, barrier-free, open access to the full text of research papers, which is in the best interests of the scientific community.

- High visibility for maximum global exposure with open access publishing model
- Rigorous peer review of research papers
- Prompt faster publication with less cost
- Guaranteed targeted, multidisciplinary audience

Scientific Research Publishing

Website: https://www.scirp.org
Subscription: sub@scirp.org
Advertisement: service@scirp.org